FACULTY
OF SCIENCE

Real-time stability and dynamics of vortices in quasi-two-dimensional self-bound two-component Bose-Einstein condensates

Philipp Stürmer

Thesis submitted for the degree of Master of Science
Project duration: 9 months, 60 hp

Supervised by Stephanie Reimann

Department of Physics
Division of Mathematical Physics
May 2019

Abstract

This thesis presents a numerical study of the beyond mean field extended Gross-Pitaevskii equation for a two-component self-bound Bose-Einstein condensate, supplemented by analytical work. We extend the quasi-two-dimensional system's mean field particle-particle contact interaction by quantum fluctuations (LHY-correction). We investigate the formation of self-bound droplets without external confinement and confirm their ground-state stability. Furthermore, we examine and discuss the real-time stability and dynamics of vortices in self-bound droplets and find a size dependence for stability and their dynamics of their release from a confined trap.

Acknowledgements

I would like to thank my supervisor, Stephanie Reimann, for her neverending patience, support and enthusiasm during this Master's thesis. Also I want to thank her for making this the most interesting and fun part for five-and-a-half years studying physics. I would also like to thank David Boholm for all the fruitful discussions we had and sometimes sacrificing the productivity in the office for an increase in fun and shenanigans. Furthermore, I thank my flatmate Izabelle Borg-Nilsson with her amazing baking skills that kept all Master students sane in periods of high-stress. I also thank Mikael Nilsson Tengstrand for writing the GPU code that ultimately led to the realisation of this thesis and proof-reading my thesis. I want to thank Gunnar Eriksson for showing me how to make animated movies of my density evolutions and proof-reading my thesis. For correcting my thesis I additionally want to thank Jakob Bengtsson, Rashi Sachdeva, Johannes Bjerlin, Oskar Schuster and Maitane Muñoz Basagoiti. Finally I thank my girlfriend Chelsea Groenhuijzen for reminding me of healthy habits in times of high stress.

List of Acronyms and Abbreviations

BEC	Bose-Einstein condensate
GPe	Gross-Pitaevskii equation
3D	Three-dimensional
Q2D	Quasi-two-dimensional
2D	Two-dimensional
LHY	Lee-Huang-Yuang

Contents

Chapter 1 | Introduction

In the 1920s Einstein and Bose predicted the condensation of an ideal atomic gas of bosonic particles into a single coherent state [1–3]. However, the realisation of Bose-Einstein condensates (BEC) was not experimentally feasible at the time. It took several decades to develop sufficiently sophisticated trapping and cooling techniques to realise Bose-Einstein condensation in ultracold atomic gases [4–8]. In the time between Einstein's and Bose's first prediction and the experimental realisation, physicists poured time and effort into developing the extensive theoretical description of condensates that we know today. Those years of theoretical work lead to the vast experimental research after the first success in 1995 and subsequent years [8–10], which makes ultracold atomic gases one of the most pursued research topics in modern physics.

In their fundamental theoretical description, ultracold atomic gases are assumed to be dilute and weakly interacting, described by the condensate's density and a scattering length. The scattering length describes the particle-particle elastic interactions and is much smaller than the average interparticle distances. This allows for a mean field description of the many-body wavefunction, turning it into a product of single-body wavefunctions. The initially complicated quantum mechanical many-body problem then reduces to that of a classical single wavefunction Hamiltonian with an additional non-linear interaction term. This treatment was first introduced, independently from each other, by Gross [11] and Pitaevskii [12]. The resulting equation has the structure of the Schrödinger equation where the interactions are approximated by a non-linear term.

As a quantum system described by a macroscopic wavefunction, the BEC cloud allows for both, classical and quantum approaches in describing its dynamics. The macroscopic wavefunction leads to treatment in classical field theory and fluid-dynamics, ultimately leading to thermodynamic properties and joint bulk motions, which are inherent macroscopic observables. However, staying in the description of second quantisation and treating the BEC via annihilation and creation operators, the energy eigenvalues of the condensate can be calculated. This quantum approach was first taken by Bogoliubov, in an attempt to formulate a theory of superfluidity [13]. Since then, both approaches have been used in many other research areas, including the calculation of Hawking-radiation of black holes [14] and a theory describing dark matter as a self-gravitating, self-interacting condensate [14].

One of the many intriguing aspects of BEC is the formation of vortices in response to rotation [15, 16]. Compared to rigid-body motion, vortices in BEC show irrotationality, which forces their density to form singularities around the centre of rotation. This is particularly interesting as it displays macroscopic effects in a condensate that only exists due to quantum effects. Furthermore, increasing the ratio of angular momentum to particle number, the number of singly quantised vortices in the gas increases, instead of a multiply quantised vortex at the trap centre [17]. If the number of vortices is high enough, this leads to grid-like structures

with discrete rotational symmetries [18]. Additionally, vortices are a sign for superfluidity and the building block for the connection between superfluidity and Bose-Einstein-condensation [15, 19, 20]. Vortices have been studied extensively in various experiments, as well as theoretically within the Gross-Pitaevskii approach [21–26].

When investigating the aforementioned dark-matter self-gravitating BEC, one finds an equilibrium between the attractive gravitational potential and the repulsive mean field interaction. In an earthbound laboratory, however, gravitational forces are too small to stabilise an untrapped condensate. However, Petrov [27] found recently, that for two-component Bose gases it is possible to find a self-bound stable solution without external confinement. This is by virtue of a higher-order correction beyond mean field, which arises to stabilise the system. The correction is due to quantum fluctuations and was first proposed by Lee, Huang and Yang and is generally referred to as the LHY-correction [28]. Only by accident physicists found that the LHY-interaction can be used to create stable self-bound droplets in one-component dipolar Bose gases [29–31]. In the case proposed by Petrov, the intraspecies repulsion of a two-component gas effectively cancels out the interspecies attraction, so that the LHY-correction stabilises the system without an external confinement. Only shortly after the initial theoretical prediction, such self-bound droplets were first found by using Feshbach resonances in two-component bosonic gases [32, 33]. Experimentally, one exploits the different dependencies of the interaction terms on the particle density and interaction parameters. Thus the interaction strengths are controlled independently, forming a droplet in equilibrium without any external trapping.

Moreover, the LHY-correction changes its physical dependence on the particle density when reducing the dimensionality of the system from three-dimensions to (quasi)-two- dimensions. Instead of only allowing for repulsive higher-order corrections, we are now also able to find attractive corrections [34, 35]. As we will see later this allows for finding stable droplets across a wider range of parameters compared to a three-dimensional system.

To the best of our knowledge, up to now, there has been no investigation whether droplets can form vortices, without assuming that the system is solved by a wavefunction containing a vortex. Thus, in this project we aim to determine whether vortices and a vortex lattice can form and sustain in a quasi-two-dimensional rotating self-bound droplet system, based on the previously mentioned beyond zeroth-order mean field extensions to the Gross-Pitaevskii equation. The analysis is done numerically using fourth- and second-order algorithms to solve the Gross-Pitaveskii equation under imaginary-time propagation, before investigating the system to address real-time stability. Such algorithms already exist for BECs within mean field and have been proven to be fast converging and accurate, with the use of Fast Fourier Transforms (FFT).

The structure of the thesis follows the structure of this introduction. Firstly we will focus on the general theoretical framework of ultra-cold dilute Bose gases by introducing Bose-Einstein condensation, followed by the Gross-Pitaevskii equation for single and two-component gases. After finishing that groundwork, we will investigate the ground state energy and LHY-correction of condensates, before analysing rotational dynamics. In the last

section of this first chapter, we will investigate the droplet formation in three-dimensions, as it resembles more natural dynamics to understand the concept entirely.

The second chapter is devoted to describe the already existing algorithm we will use to solve the following systems. We introduce the algorithm by first solving the quantum mechanical harmonic oscillator, before displaying the Gross-Pitaveskii equation as a harmonic oscillator. As such algorithm was designed to solve a particle in a magnetic field, we need to create a bridge between the proposed system and the Gross-Pitaevskii equation with external rotation.

In the last theoretical chapter, the previously introduced system is squeezed from three-dimensions to a quasi-two-dimensional system. We will discuss the mean field interaction independently from the LHY-correction and explain why the vortex formation is independent of the dimensionality.

The last chapter is dedicated to results, where we first show the formation of droplets in quasi-two-dimensions, without external confinement. We continue by rotating stable solutions in a trap and compare it to the formation of quantised vortices in a trapped mean field condensate. As a last part we rotate stable solutions in a trap, before releasing it in real-time. We then investigate the real-time stability and dynamics of singly quantised and multiple single quantised systems.

Chapter 2 | Bose Einstein condensation (BEC)

The BEC is the fundamental phenomenon discussed throughout this thesis. This chapter is dedicated to exploring the creation and behaviour of a condensate. Firstly, we will provide a brief overview of Bose-Einstein condensation. Secondly, in Sec. 2.2 we introduce the Gross-Pitaevskii equation, motivated by a second-quantisation approach. This will give a partial differential equation describing the evolution of the condensate, governed by contact interactions. The Gross-Pitaevskii equation (GPe) will then be investigated in Sec. 2.3, focusing on its energy and rotational behaviour, to build a foundation for the discussion about self-bound droplets in two-component Bose-gas.

2.1 Bose-Einstein condensation

Particles on the atomic and sub-atomic level are divided into two groups, Bosons and Fermions. Following the spin-statistics theorem, Bosons have integer spin, for which the wavefunction of identical bosons is symmetric under exchange of parity on any two particles [36]. Fermions, however, have half-integer spin, where the wavefunction of identical fermions becomes antisymmetric under use of parity on any two particles. This symmetry leads directly to the Pauli-exclusion principle for Fermions. For non-interacting Bosons, the symmetry implies that an indefinite number of bosons may occupy the same single-particle state. This behaviour was first predicted by Bose for light quanta and later generalised by Einstein for any particle with bosonic properties [1–3].

The condensation of Bosons is governed by Bose-Einstein statistics, which can be displayed by the Bose-Einstein distribution (see e.g. [37]). The average expected number of particles $\langle n_i(E_i)\rangle$ in an energy state i with energy E_i of a given system of Bosons is given by

$$\langle n_i(E_i)\rangle = \frac{1}{e^{(E_i-\mu)}/(k_B T) - 1}, \tag{2.1}$$

with μ the chemical potential, k_B the Boltzmann-constant, T the temperature, and $E_i > \mu$ at all times. We immediately see that for $(E_i - \mu) \to 0$ the occupation number reaches infinity. Thus all particles condense into the same single-particle state.

Expressing the field in the second quantisation notation $\hat{\Psi}$, consisting of position eigenstates $\phi_i(\mathbf{r})$ and their respective annihilation operators $\hat{a}_i$,

$$\hat{\Psi}(\mathbf{r}) = \sum_{i=0} \phi_i(\mathbf{r})\hat{a}_i.$$

Further, we want to decompose the second quantisation operator in its ground state ϕ_0 and higher energy states

$$\hat{\Psi}(\mathbf{r}) = \phi_0(\mathbf{r})\hat{a}_0 + \sum_{i\neq 0} \phi_i(\mathbf{r})\hat{a}_i. \tag{2.2}$$

Given a system's total particle number N and the number of condensed particles N_0, we can assume that the system is fully condensed when $N_0 \to N$. This allows for the use of the so called Bogoliubov approximation [13, 38] $\langle \hat{a}_0^\dagger \hat{a}_0 \rangle \approx N_0$, hence $\hat{a}_0 \approx \sqrt{N_0}$, where $\hat{a}_0^\dagger$ and $\hat{a}_0$ are the single state creation and annihilation operators, respectively. Additionally, the Bogoliubov approximation requires that the condensate consists of a sufficiently high particle number, so that commutation becomes negligible, i.e. $[\hat{a}_0^\dagger, \hat{a}_0] = 0$. Inserting $\hat{a}_0 \approx \sqrt{N_0}$ into Eq. (2.2) gives

$$\hat{\Psi}(\mathbf{r}) = \sqrt{N_0}\phi_0(\mathbf{r}) + \delta\hat{\Psi}(\mathbf{r}). \tag{2.3}$$

Considering a pure condensate, where all Bosons are in $\phi_0(\mathbf{r})$ and thus omitting the second term, turns the second quantisation operator into a classical field. Explicitly, this means that we can describe a system governed by quantum effects in a classical manner [38].

2.2 Gross-Pitaevskii equation (GPe)

In this section we will derive the GPe, with the second quantisation field-operator $\hat{\Psi}(\mathbf{r}, t)$, whith the details given in App. (A). The Gross-Pitaveskii equation has been proven to be successful in describing BECs numerically [12, 38, 39]. Thus, it will be our main tool for this thesis. The field operator $\hat{\Psi}(\mathbf{r}, t)$ in the Heisenberg picture fulfills [38]

$$\begin{aligned} i\hbar\frac{\partial}{\partial t}\hat{\Psi}(\mathbf{r},t) &= \left[\hat{\Psi}(\mathbf{r},t), \hat{H}\right] \\ &= \left[-\frac{\hbar^2\boldsymbol{\nabla}^2}{2m} + V_{ext}(\mathbf{r},t) + \int d\mathbf{r}'\, \hat{\Psi}^\dagger(\mathbf{r}',t)V(\mathbf{r}'-\mathbf{r},t)\hat{\Psi}(\mathbf{r}',t)\right]\hat{\Psi}(\mathbf{r},t). \end{aligned} \tag{2.4}$$

Eq. (2.4) can be attained when using the many-body Hamiltonian $\hat{H}$, expressed in the second quantisation field-operator $\hat{\Psi}(\mathbf{r}, t)$

$$\hat{H} = \int d\mathbf{r}\, \left(\frac{\hbar^2}{2m}\boldsymbol{\nabla}\hat{\Psi}^\dagger(\mathbf{r},t)\boldsymbol{\nabla}\hat{\Psi}(\mathbf{r},t)\right) + \frac{1}{2}\int d\mathbf{r}' d\mathbf{r}\, \hat{\Psi}^\dagger(\mathbf{r},t)\hat{\Psi}^\dagger(\mathbf{r}',t)V\left(\mathbf{r}'-\mathbf{r},t\right)\hat{\Psi}(\mathbf{r},t)\hat{\Psi}(\mathbf{r}',t), \tag{2.5}$$

where the factor $1/2$ rises to account for a single interaction between $\Psi(\mathbf{r}, t)$ and $\Psi(\mathbf{r}', t)$ and to avoid double-counting. We yield Eq. (2.5) with the commutation relations

$$\left[\hat{\Psi}(\mathbf{r},t), \hat{\Psi}^\dagger(\mathbf{r}',t)\right] = \delta(\mathbf{r}-\mathbf{r}') \text{ and} \tag{2.6}$$

$$\left[\hat{\Psi}(\mathbf{r},t), \hat{\Psi}(\mathbf{r}',t)\right] = 0. \tag{2.7}$$

and $\hat{\Psi}(\mathbf{r},t)$ given in terms of the annihilation and creation operator $\hat{a}_{\mathbf{p}}$, $\hat{a}^{\dagger}_{\mathbf{p}}$ [38]

$$\hat{\Psi}(\mathbf{r},t) = \sum_{\mathbf{p}} \hat{a}_{\mathbf{p}} \frac{1}{\sqrt{V}} \exp\left(\frac{i\mathbf{p}\cdot\mathbf{r}}{\hbar}\right). \tag{2.8}$$

The remaining integral in Eq. (2.4) is not solvable by perturbation theory for a realistic hard-sphere contact potential. This is generally dealt with by using the diluteness criteria $na_s^{1/3} \ll 1$. Here n is the particle density and a_s the s-wave scattering length. If the bosonic gas fulfills $na_s^{1/3} \ll 1$, the inter-particle distance is big enough that the exact form of contact potential at its centre becomes irrelevant. Thus the potential shape is interchangeable, as long as it preserves a_s. Exchanging the hard-sphere potential with an effective soft potential that shares the same s-wave scattering length a_s, allows to separate the potential from the field operator, thus turning the integral into $g|\Psi(\mathbf{r},t)|^2$ with $g = \int V(\mathbf{r})\, d\mathbf{r}$ expressed using the scattering length a_s as $g = 4\pi\hbar^2 a_s/m$ [38].

Following Eq. (2.3), we replace the field operator by a classical order parameter $\Psi_0(\mathbf{r},t)$. This only applies when $\delta\hat{\Psi}(\mathbf{r}) \to 0$ and thus then the temperature of the condensate $T \to 0$. The final Gross-Pitaveskii equation shows similarity to the non-linear Schrödinger equation and is then given by [38]:

$$i\hbar\frac{\partial}{\partial t}\Psi_0(\mathbf{r},t) = \left(-\frac{\hbar^2\nabla^2}{2m} + V_{ext}(\mathbf{r},t) + g|\Psi_0(\mathbf{r},t)|^2\right)\Psi_0(\mathbf{r},t). \tag{2.9}$$

It is important to put emphasis on the applicability of this approach. First, we need a sufficient amount of atoms, so that we are allowed to treat the system as a BEC. Second, the diluteness condition needs to be fulfilled, and the temperature must be low enough to replace the actual potential with an effective potential and the field operator with the order parameter. Under these conditions and from the Bogoliubov approximation in the previous section follows that

$$n(\mathbf{r}) = |\Psi_0(\mathbf{r})|^2. \tag{2.10}$$

We can easily extend the single-component equation Eq. (2.9) to a multi-component Gross-Pitaevskii equation. For a two-component bosonic system with equal masses this gives us

$$i\hbar\frac{\partial}{\partial t}\Psi_{0,1}(\mathbf{r},t) = \left(-\frac{\hbar^2\nabla^2}{2m} + V_{ext}(\mathbf{r},t) + g_{11}|\Psi_{0,1}(\mathbf{r},t)|^2 + g_{12}|\Psi_{0,2}(\mathbf{r},t)|^2\right)\Psi_{0,1}(\mathbf{r},t), \tag{2.11}$$

$$i\hbar\frac{\partial}{\partial t}\Psi_{0,2}(\mathbf{r},t) = \left(-\frac{\hbar^2\nabla^2}{2m} + V_{ext}(\mathbf{r},t) + g_{22}|\Psi_{0,2}(\mathbf{r},t)|^2 + g_{21}|\Psi_{0,1}(\mathbf{r},t)|^2\right)\Psi_{0,2}(\mathbf{r},t) \tag{2.12}$$

where g_{ij} is the interaction parameter between particle species i and j, $\Psi_{0,i}$ the order parameter of particle species i. Furthermore, we see that the effective external potential V_{ext} can represent any form of additional potential.

2.3 Energy of the dilute Bose gas

In this section, we will find the energy eigenvalues of our dilute bosonic gas Hamiltonian, in the ground state described by the mean field interaction as well as the first higher order

correction to the mean field description. In doing so, we will use an approach first utilised by Bogoliubov, which will yield the ground state energy for a system of quasi-particles in the case of the first higher order correction.

2.3.1 Ground state energy of the dilute Bose gas

To calculate the ground state energy we use the Hamiltonian in Eq. (2.5) and insert the following second quantisation operator $\hat{\Psi}$ and two-body interaction potential $\mathbf{V_q}$, [38, 39]

$$\hat{\Psi} = \sum_{\mathbf{p}} \hat{a}_{\mathbf{p}} \frac{1}{\sqrt{V}} \exp\left(\frac{i\mathbf{p}\cdot\mathbf{r}}{\hbar}\right),$$
$$V_{\mathbf{q}} = \int d\mathbf{r}\, V(\mathbf{r}) \exp\left(\frac{-i\mathbf{q}\cdot\mathbf{r}}{\hbar}\right),$$

into Eq. (2.5), which gives

$$\hat{H} = \sum \frac{p^2}{2m} \hat{a}^\dagger_{\mathbf{p}} \hat{a}_{\mathbf{p}} + \frac{1}{2V} \sum V_{\mathbf{q}} \hat{a}_{\mathbf{p}_1+\mathbf{q}} \hat{a}^\dagger_{\mathbf{p}_2-\mathbf{q}} \hat{a}_{\mathbf{p}_1} \hat{a}_{\mathbf{p}_2}, \tag{2.13}$$

with V being the volume of the system, $V_{\mathbf{q}}$ the two-body interaction potential and the first summation over $\mathbf{p}$ and the second over $\mathbf{p}_1$, $\mathbf{p}_2$, and $\mathbf{q}$ [38]. Here $\mathbf{p}$ is the particle's linear momentum without $V_{\mathbf{q}}$ the interaction potential, $\mathbf{p}_1$, $\mathbf{p}_2$, the respective particle's linear momentum before collision and $\mathbf{q}$ the linear momentum exchange. Again, we interchange the actual contact particle-particle interaction potential $V_{\mathbf{q}}$ with a Gaussian shaped pseudopotential, thus resulting in an interaction parameter U_0 as long as $na^{1/3} \ll 1$ is fulfilled.

$$\hat{H} = \sum \frac{p^2}{2m} \hat{a}^\dagger_{\mathbf{p}} \hat{a}_{\mathbf{p}} + \frac{1}{2V} U_0 \sum \hat{a}_{\mathbf{p}_1+\mathbf{q}} \hat{a}^\dagger_{\mathbf{p}_2-\mathbf{q}} \hat{a}_{\mathbf{p}_1} \hat{a}_{\mathbf{p}_2}. \tag{2.14}$$

Assuming that all particles in the system are in the ground state at zero temperature, with $N_0 = N$ and thus $\langle \hat{a}^\dagger_0 \hat{a}_0 \rangle = N_0$, allows for the Bogoliubov approximation $\hat{a}_0 = \sqrt{N_0}$ [13]

$$\hat{H} = \sum \frac{p^2}{2m} \hat{a}^\dagger_0 \hat{a}_0 + \frac{1}{2V} U_0 \sum \hat{a}^\dagger_0 \hat{a}^\dagger_0 \hat{a}_0 \hat{a}_0.$$

The first term equals zero with $\mathbf{p} = 0$ and thus, the ground state energy becomes

$$E_0 = \frac{N^2 U_0}{2V}, \tag{2.15}$$

with $U_0 = 4\pi\hbar^2 a_s/m$, where a_s is the three-dimensional s-wave scattering length of the pseudo potential, obtained from the Born approximation. Physical systems are frequently described by the interaction coupling constant $g = 4\pi\hbar^2 a_s/m$ [38].

2.3.2 First order correction to the energy

The previous approximation, where the condensate is at $T = 0$, and thus $\mathbf{p} = \mathbf{p}_1 = \mathbf{p}_2 = \mathbf{q} = 0$, is not applicable for realistic physical systems, where some particles lie in an excited

state, thus resulting in non-negligible linear momentum contributions $\mathbf{p} \neq 0$ [13]. Starting off from revisiting Eq. (2.14), we make the approximation of a soft pseudo-potential. Due to the conservation of linear momentum, terms with only one operator $\mathbf{p} \neq 0$ are not possible [38]. We write the Hamiltonian again, but with the ground state energy already excluded, in order to calculate the first order correction to the energy:

$$\hat{H} = \frac{U_0}{2V}\hat{a}_0^\dagger\hat{a}_0^\dagger\hat{a}_0\hat{a}_0 + \sum_{\mathbf{p}} \frac{p^2}{2m}\hat{a}_{\mathbf{p}}^\dagger\hat{a}_{\mathbf{p}} + \frac{U_0}{2V}\sum_{\mathbf{p}\neq 0}\left(4\hat{a}_0^\dagger\hat{a}_{\mathbf{p}}^\dagger\hat{a}_0\hat{a}_{\mathbf{p}} + \hat{a}_{\mathbf{p}}^\dagger\hat{a}_{-\mathbf{p}}^\dagger\hat{a}_0\hat{a}_0 + \hat{a}_0^\dagger\hat{a}_0^\dagger\hat{a}_{-\mathbf{p}}\hat{a}_{-\mathbf{p}}\right). \tag{2.16}$$

Here the first term represents the already known ground state energy Eq. (2.15) for particles in the condensate. The second term represents the kinetic energy contribution and the third term the ground state energy for particles in the condensate with nonzero linear momentum. The factor four in the first part of the third term derives from simple combinatorics of indistinguishable particles.

We replace the zero momentum components in the third term with $\hat{a}_0 = \sqrt{N_0}$, while in the first term we use quadrature of the sum over all states $\hat{a}_0^\dagger\hat{a}_0 + \sum_{\mathbf{p}\neq 0}\hat{a}_{\mathbf{p}}^\dagger\hat{a}_{\mathbf{p}} = N$, also called the renormalisation relation:

$$\hat{a}_0^\dagger\hat{a}_0^\dagger\hat{a}_0\hat{a}_0 = N^2 - 2N\sum_{\mathbf{p}\neq 0}\hat{a}_{\mathbf{p}}^\dagger\hat{a}_{\mathbf{p}} + \left(\sum_{\mathbf{p}\neq 0}\hat{a}_{\mathbf{p}}^\dagger\hat{a}_{\mathbf{p}}\right)^2, \tag{2.17}$$

where we can neglect higher order terms in brackets $\mathbf{p} \neq 0$, due to their small contribution [38]. Unfortunately, the substitution of the real interaction matrix element V_q by the pseudopotential and constant value U_0 results in a divergence. This is counteracted in the literature by replacing U_0 with the higher-order dependency of the interaction coupling constant g according to higher-order perturbation theory.

$$U_0 = g\left(1 + \frac{g}{V}\sum_{\mathbf{p}\neq 0}\frac{m}{p^2}\right). \tag{2.18}$$

Substituting the renormalisation relation in Eq. (2.17) and Eq. (2.18) into Eq. (2.16), yields the following expression [38]

$$\hat{H} = g\frac{N^2}{2V} + \sum \frac{p^2}{2m}\hat{a}_{\mathbf{p}}^\dagger\hat{a}_{\mathbf{p}} + \frac{1}{2}gn\sum_{\mathbf{p}\neq 0}\left(2\hat{a}_{\mathbf{p}}^\dagger\hat{a}_{\mathbf{p}} + \hat{a}_{\mathbf{p}}^\dagger\hat{a}_{-\mathbf{p}}^\dagger + \hat{a}_{\mathbf{p}}\hat{a}_{-\mathbf{p}} + \frac{mgn}{p^2}\right). \tag{2.19}$$

The quadratic dependency of the Hamiltonian on the operators $\hat{a}_{-\mathbf{p}}^\dagger$ and $\hat{a}_{\mathbf{p}}$, allows for diagonalisation by the linear transformation known as the Bogoliubov transformation [13],

$$\hat{a}_{\mathbf{p}} = u_{\mathbf{p}}\hat{b}_{\mathbf{p}} + v_{-\mathbf{p}}^*\hat{b}_{-\mathbf{p}}^\dagger, \quad \hat{a}_{\mathbf{p}}^\dagger = u_{\mathbf{p}}^*\hat{b}_{\mathbf{p}}^\dagger + v_{-\mathbf{p}}\hat{b}_{-\mathbf{p}}, \tag{2.20}$$

where $\hat{b}_{\mathbf{p}}^\dagger$ and $\hat{b}_{\mathbf{p}}$ are the new quasiparticle operators [13, 38]. These operators share the Bose commutation relations with the original particle operators $\hat{a}_{\mathbf{p}}^\dagger$ and $\hat{a}_{\mathbf{p}}$, i.e. $\hat{a}_{\mathbf{p}}\hat{a}_{\mathbf{p}'}^\dagger - \hat{a}_{\mathbf{p}'}^\dagger\hat{a}_{\mathbf{p}} = \delta_{\mathbf{p}\mathbf{p}'}$. Using the commutation relationship with the Bogoliubov transformation, we get

$$|u_{\mathbf{p}}|^2 - |v_{-\mathbf{p}}|^2 = 1 \tag{2.21}$$

and after algebraic manipulation (App. (C)), we find the diagonalised Hamiltonian

$$\hat{H} = E_0 + \sum \epsilon(\mathbf{p}) \hat{b}^\dagger_{\mathbf{p}} \hat{b}_{\mathbf{p}}, \tag{2.22}$$

with

$$E_0 = g\frac{N^2}{2V} + \frac{1}{2}\sum_{\mathbf{p}\neq 0}\left[\epsilon(\mathbf{p}) - gn - \frac{p^2}{2m} + \frac{m(gn)^2}{p^2}\right], \tag{2.23}$$

being the ground state energy to the higher order approximation and

$$\epsilon(\mathbf{p}) = \left[\frac{gn}{m}p^2 + \left(\frac{p^2}{2m}\right)^2\right]^{1/2} \tag{2.24}$$

is the dispersion relation of the excitations [38].

This shows that the original system of interacting particles can be described in terms of a Hamiltonian of quasi-particles with ground state energy E_0. From their respective annihilation and creation operators $\hat{b}_{\mathbf{p}}$ and $\hat{b}^\dagger_{\mathbf{p}}$, the original bosonic particles can be understood as two quasi-particles propagating in opposite directions. Considering Eq. (2.17), we recognise that the quadratic terms of operators can be understood as the creation and annihilation of quasi-particles in the same operation. Thus one often refers to the higher-order energy correction as an energy shift due to quantum fluctuations.

To calculate the ground state energy E_0 we turn the sum over the phase space in Eq. (2.23) into a phase space integral (App. (C)), which yields the result [38, 40]

$$E_0 = g\frac{N^2}{2V}\left[1 + \frac{128}{15\sqrt{\pi}}(na^3)^{1/2}\right], \tag{2.25}$$

where the first term is the mean field ground state energy, calculated in the previous section and the second term gives the higher order correction. This calculation was first done by Lee, Huang and Yang in 1957 and is thus called the LHY-correction. However, Eq. (2.25) gives the correction term in case of a three-dimensional spherical system for a single-component bosonic gas. Thus, it is not reasonable to use it in the case of this thesis, as we want to study a two-component Bose-gas in quasi-two-dimensions. The three-dimensional case, however, illustrates the general physical behaviour and is worth studying in itself. Larsen did a similar calculation for a two-component Bose-gas [41] and the LHY-correction is then given in a similar form by

$$E_{LHY} = V\frac{32\sqrt{2\pi}}{15}\sum_{\pm}\left(a_{11}n_1 + a_{22}n_2 \pm \kappa\right)^{5/2}, \tag{2.26}$$

with $\kappa = \left[\left(a_{11}n_1 - a_{22}n_2\right)^2 + 4a_{12}^2 n_1 n_2\right]^{1/2}$, a_{ij} the s-wave scattering length between component i and j and n_i is the density distribution for component i. For $a_{12} = -\sqrt{a_{11}a_{22}}$ Eq. (2.26) gives

$$E_{LHY} = V\frac{256}{15}\sqrt{\pi}\left(a_{11}n_1 + a_{22}n_2\right)^{5/2}. \tag{2.27}$$

A quasi-two-dimensional solution to the LHY-correction was done only recently by Zin [35] and Ilg [42], which we will further investigate in Ch. 4 about dimensional reduction.

2.4 Rotational dynamics of a dilute Bose gas in the mean field description

An important feature of BECs is the formation of quantised vortices under rotation, as it exemplifies the connection between superfluidity and Bose-Einstein condensation [19, 20]. Thus, we will investigate the rotational dynamics of a dilute Bose-gas, by first deriving the continuity equation of the GPe and then introducing the current density $\mathbf{j}$ and flow velocity $\mathbf{v}$. We then use the flow velocity to elaborate on the concept of irrotationality. Further investigation will include the structure, energy and critical angular momentum of quantised vortices, for a rotating condensate with external rotation frequency Ω.

We derive the continuity equation by following the well known formalism from classical field theory. Multiplying Eq. (2.9) with Ψ_0^* and subtracting the complex conjugate of the resulting equation from itself, gives [38, 39]:

$$\frac{\partial|\Psi_0(\mathbf{r},t)|^2}{\partial t} - \frac{i\hbar}{2m}\boldsymbol{\nabla}\left((\Psi_0^*(\mathbf{r},t)\boldsymbol{\nabla}\Psi_0(\mathbf{r},t) - \Psi_0(\mathbf{r},t)\boldsymbol{\nabla}\Psi_0^*(\mathbf{r},t))\right) = 0. \tag{2.28}$$

We then introduce the current density $\mathbf{j}$ as given by,

$$\mathbf{j}(\mathbf{r},t) = -\frac{i\hbar}{2m}\left(\Psi_0^*(\mathbf{r},t)\boldsymbol{\nabla}\Psi_0(\mathbf{r},t) - \Psi_0(\mathbf{r},t)\boldsymbol{\nabla}\Psi_0^*(\mathbf{r},t)\right). \tag{2.29}$$

Inserting Eq. (2.29) into Eq. (2.10), the continuity equation in Eq. (2.28) reduces to

$$\frac{\partial n}{\partial t} + \operatorname{div}\mathbf{j}(\mathbf{r}) = 0. \tag{2.30}$$

The flow velocity $\mathbf{v}(\mathbf{r})$ of the condensate is then defined by $\mathbf{j}(\mathbf{r}) = n\mathbf{v}(\mathbf{r})$. We now rewrite the order parameter $\Psi_0(\mathbf{r})$ with it's density amplitude and a phase S

$$\Psi_0(\mathbf{r}) = \sqrt{n(\mathbf{r})}e^{iS(\mathbf{r})} = |\Psi_0(\mathbf{r})|e^{iS(\mathbf{r})}. \tag{2.31}$$

Thus, Eq. (2.29) and $\mathbf{v}$ become

$$\begin{aligned}\mathbf{j}(\mathbf{r}) &= n\frac{\hbar}{m}\boldsymbol{\nabla}S(\mathbf{r}),\\ \mathbf{v}(\mathbf{r}) &= \frac{\hbar}{m}\boldsymbol{\nabla}S(\mathbf{r}).\end{aligned} \tag{2.32}$$

To determine the condensate's dynamics under rotation we apply $\boldsymbol{\nabla}\times$:

$$\boldsymbol{\nabla}\times\mathbf{v}(\mathbf{r}) = \frac{\hbar}{m}\boldsymbol{\nabla}\times\boldsymbol{\nabla}S(\mathbf{r}) = 0. \tag{2.33}$$

Without loss of generality we bring the condensate into cylindrical coordinates, where the density only depends on the radius r and the height z, while only the phase factor depends on ϕ:

$$\Psi_0(r, z, \phi) = |\Psi_0(r, z)|e^{i\phi}. \tag{2.34}$$

With Eq. (2.32) and $\boldsymbol{\nabla}$ in cylindrical coordinates, $\mathbf{v}$ then becomes

$$\mathbf{v}(\mathbf{r}) = \frac{\hbar}{m}\frac{1}{r}\hat{\mathbf{e}}_\phi. \tag{2.35}$$

Eq. (2.33) and (2.35) classify a fluid as irrotational, where the flow velocity changes $1/r$ from the center; compared to the rotation of a rigid body, where it increases linearly with the distance from its center. With that irrotationality and the introduction of the phase factor follow two conclusions. Firstly, due to the $1/r$ dependence of the velocity, $\mathbf{v}$ would diverge in the center of the condensate. Thus we impose that the density $|\Psi_0(r, z)| \to 0$ as $r \to 0$. Secondly, should there be no change in the wavefunction after rotating for 2π, $\Psi_0(r, z, \phi) = \Psi(r, z, \phi + 2\pi)$, thus [38, 39]

$$\Delta S = \oint d\mathbf{l}\, \boldsymbol{\nabla} S = 2\pi l, \tag{2.36}$$

with l an integer, which gives the rotational quantisation of the condensate, which we reintroduce into Eq. (2.34)

$$\Psi_0(r, z, \phi) = |\Psi_0(r, z)|e^{il\phi}. \tag{2.37}$$

From the previous discussion, we see that the condensate's rotation will lead to a singularity in its density in the centre of the rotation. We see that the rotation always associates with a phase jump in it's phase factor $\exp(il\phi)$ [38, 39].

Further, we will calculate the energy of singly and multiply, i.e. $l > 1$, quantised vortices, as well as the critical angular momentum, that associates with the existence of vortices. The energy expectation value of a condensate's Hamiltonian without an external potential is governed by the kinetic term and the zeroth-order interaction therm, thus resulting in [38, 39]

$$E = \int d\mathbf{r} \left[\frac{\hbar}{2m}|\boldsymbol{\nabla}\Psi_0(\mathbf{r})|^2 + \frac{1}{2}U_0|\Psi_0(\mathbf{r})|^4\right]. \tag{2.38}$$

Returning to our system in cylindrical coordinates, and imposing z-coordinate invariance, the energy of a condensate with a vortex of rotational quantisation l is then given by

$$E = \int_0^R dr\, 2\pi r \left[\frac{\hbar}{2m}\left(\frac{\partial|\Psi_0(\mathbf{r})|}{\partial r}\right)^2 + \frac{\hbar}{2m}l^2\frac{|\Psi_0(\mathbf{r})|^2}{r^2} + \frac{U_0}{2}|\Psi_0(r)|^4\right], \tag{2.39}$$

from the center of the vortex to a distance R. In order to calculate the energy associated with a vortex in a uniform, untrapped condensate, we subtract the ground state energy from

Eq. (2.39). The total number of particles in a 2-dimensional cylindrical volume is given by [38, 39]

$$N = \int_0^R dr\, r 2\pi |\Psi_0(r)|^2 = \pi R^2 |\Psi_0(R)|^2 - \int_0^R dr\, 2\pi r \left(|\Psi_0(R)|^2 - |\Psi_0(r)|^2 \right), \tag{2.40}$$

with the ground state energy per particle $E_0 = (1/2)U_0|\Psi_0|^4$, and the condensate's ground state energy $\mathcal{E}_0$ is then

$$\begin{aligned} \mathcal{E}_0 &= \frac{1}{2} U_0 \int_0^R dr\, r |\Psi_0(r)|^4 \\ &= \frac{1}{2}\pi R^2 |\Psi_0(R)|^4 - |\Psi_0(R)|^4 U_0 \int_0^R 2\, dr\, \pi r (|\Psi_0(R)|^2 - |\Psi_0(r)|^2). \end{aligned} \tag{2.41}$$

Introducing $|\Psi_0| = \sqrt{n} f(\eta)$ and $\eta = r/\xi$ with $\xi = \hbar/\sqrt{2mgn}$, the so called healing length of the condensate. The healing length gives the distance over which the wavefunction tends to its bulk value from zero in the case of being trapped in an infinite well. Using both substitutions gives for the total energy of a vortex $\mathcal{E}_v$:

$$\mathcal{E}_v = \frac{\pi \hbar^2 n}{m} \int_0^{R/\xi} d\eta \left[\left(\frac{df}{d\eta} \right)^2 + \frac{l^2}{\eta^2} f^2 + \frac{1}{2}(f^2 - 1)^2 \right] \eta. \tag{2.42}$$

For $l = [1, 2, 3]$ via numerical integration this gives [43]

$$\begin{aligned} \mathcal{E}_{v,l=1} &= \pi n \frac{\hbar^2}{m} \ln\left(\frac{1.46R}{\xi} \right), \\ \mathcal{E}_{v,l=2} &= 4\pi n \frac{\hbar^2}{m} \ln\left(\frac{0.59R}{\xi} \right), \\ \mathcal{E}_{v,l=3} &= 9\pi n \frac{\hbar^2}{m} \ln\left(\frac{0.38R}{\xi} \right). \end{aligned} \tag{2.43}$$

Further, one can show that it is energetically favourable for a vortex with $l > 1$ to split up in several single-quantised vortices. However, vortices with multiple quanta of circulation can be energetically favourable in anharmonic trapping potentials [44, 45].

Treating the condensate as a uniform medium, we can compute the total angular momentum, as the sum of each particles angular momentum, so that with $\mathcal{E}_{v,l=1} = \Omega_c \mathcal{L}$

$$\mathcal{L} = N\hbar,$$

such that

$$\Omega_c = \frac{\hbar}{mR^2} \ln\left(\frac{1.46R}{\xi} \right), \tag{2.44}$$

with Ω_c the critical rotation needed for it to be energetically favourable of a single quantised vortex to enter the condensate [38, 39]. So far we investigated a condensate as a

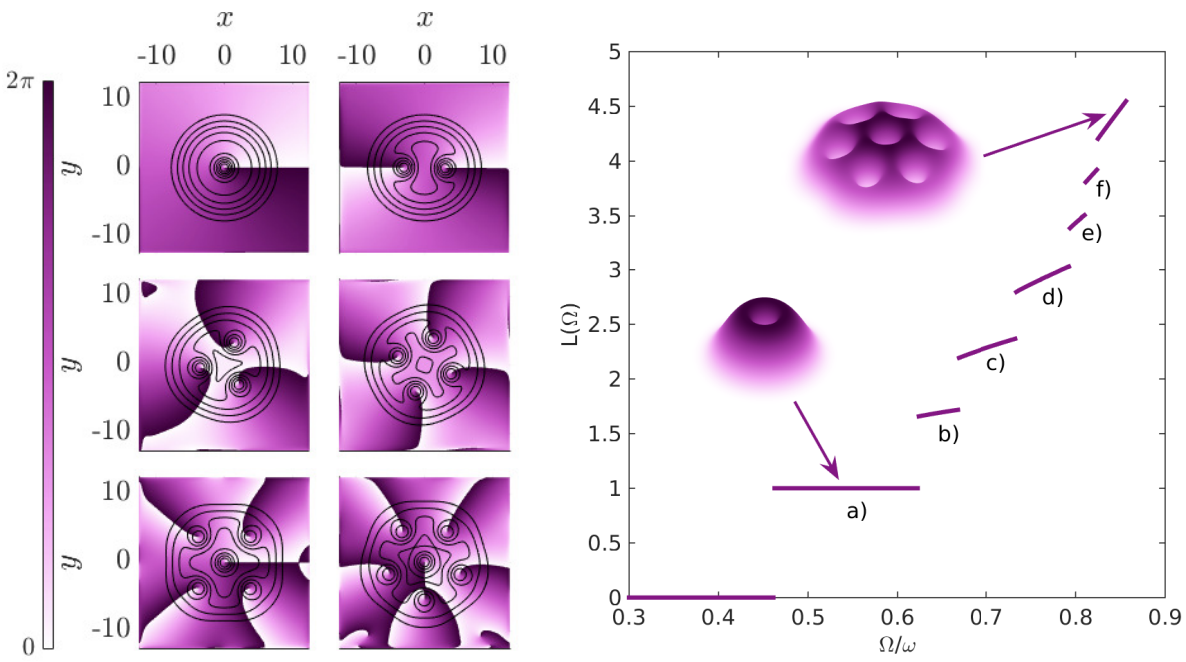

Figure 2.1: Left: Condensate density distributions as indicated by the labels, with their respective phase plotted in the background. We see the existence of phase discontinuities localised within the density-singularity.
Right: $L(\Omega/\omega)$ for mean field interaction $g = 50$ and $\omega = 0.1$, where $L(\Omega/\omega)$ is the angular momentum per particle in dependence of the ratio between external rotation Ω and the harmonic oscillator frequency ω. We see the existence of critical angular momentum, which leads to a phase-transition between higher states of vorticity.

uniform medium, without any external trapping potential. We want to repeat the calculation following from Eq. (2.39) for a two-dimensional one-component condensate trapped in a two-dimensional harmonic oscillator with oscillator frequency ω. If the traps oscillator length a_{osc} is large compared to the healing length ξ, we can calculate the energy by using Eq. (2.43) up to a radius r_1 and then calculate the energy for $r_1 < r < R$ in a classical way. This gives [46]:

$$\mathcal{E}_v = \frac{\pi n\hbar}{m} \ln\left(\frac{1.46R}{\xi}\right) + \frac{1}{2}\int_{r_1}^{R} dr\, mn(r)v^2(r)2\pi r. \tag{2.45}$$

With the density inside of a trap in the Thomas-Fermi approximation, where the interaction strength is so big, that the kinetic contribution is negligible, taking the form $1 - r^2/R^2$ and the velocity v given in magnitudes of $\hbar/mr$. Eq. (2.45) then computes to

$$\begin{aligned} \mathcal{E}_v &= \frac{\pi n\hbar}{m}\left[\ln\left(\frac{1.46R}{\xi}\right) + \int_{r_1}^{R} dr\,\frac{r}{r^2}\left(1 - \frac{r^2}{R^2}\right)\right] = \\ &= \frac{\pi n\hbar}{m}\ln\left(\frac{0.888R}{\xi}\right). \end{aligned} \tag{2.46}$$

We now repeat the calculation of the total angular momentum, by integrating over the density distribution:

$$\begin{aligned}\mathcal{L} &= n_0\hbar \int_0^R dr \left(1 - \frac{r^2}{R^2}\right) 2\pi r \\ &= \frac{1}{2} n_0 \pi R^2 \hbar\end{aligned}$$

which then gives the critical angular momentum Ω_c, with $a_{osc} = \sqrt{\hbar/m\omega}$ [46]

$$\Omega_{c,l=1} = 2\omega \frac{a_{osc}^2}{R^2} \ln\left(\frac{0.888R}{\xi}\right). \tag{2.47}$$

In Fig. (2.1, left) we plotted the density as contour over the phase in the background for a one-component BEC trapped in $\omega = 0.1$ with $g = 50$, while in Fig. (2.1, right) the respective $L(\Omega/\omega)$ plot is shown, where $L(\Omega/\omega)$ is the angular momentum per particle in dependence of the ratio between external rotation Ω and the harmonic oscillator frequency ω. Firstly, we can can confirm the existence of a critical angular momentum, due to the discrete jumps in $L(\Omega/\omega)$. Furthermore, we recognise the preference of multiple single-quantised vortices over one multiple-quantised one for a harmonic trap in Fig. (2.1, left), as indicated by the phase in the background. As previously derived, each phase discontinuity corresponds to a singularity in the condensate's density.

2.5 Self-bound droplets in three-dimensions

So far we have looked at zeroth-order mean field interaction and the first-order LHY-correction. Let us now investigate how those cooperate with each other in a physical system. We are particularly interested in forming a self-bound two-component system, which was first predicted by Petrov [27]. This section follows [27], where we will first investigate the formation of those self-bound droplets before discussing their geometry.

We introduce δg, which will be defined as

$$\delta g = g_{12} + \sqrt{g_{11} g_{22}}, \tag{2.48}$$

with g_{ij} defined as in Ch. 2.2. We then investigate how the zeroth-order mean field energy of the given system changes, which is given by,

$$E_{MF,i} = g_{ii} \frac{N^2}{2V} + g_{12} \frac{N^2}{2V},$$

for component $i = 1, 2$ with Eq.(2.48) and $g_{11} = g_{22} = g$ follows

$$E_{MF} = \delta g \frac{N^2}{2V}. \tag{2.49}$$

Thus, without taking quantum fluctuations into account, the system will be driven apart for $\delta g \geq 0$ and collapse for $\delta g < 0$. The formation of self-bound droplets in the absence of

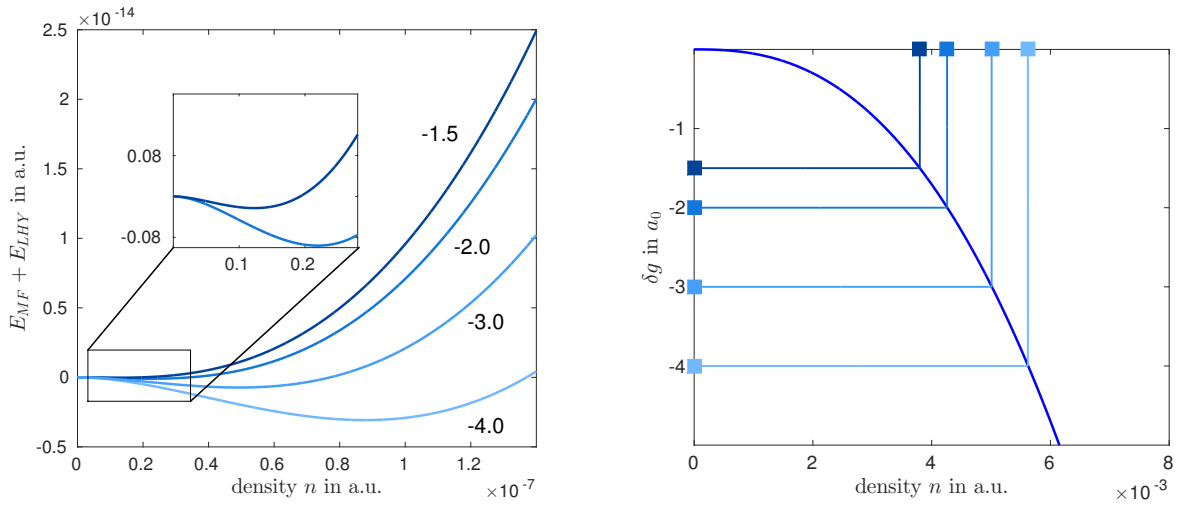

Figure 2.2: Left: $E_{MF}+E_{LHY}$ for different δg in the range from -4.0 to -1.5, based on Eq. (2.26). As we approach $\delta g \to 0$, the negative bulge in energy vanishes, as indicated by the zoom-in for $\delta g = [-1.5, -2.0]$.
Right: $\delta g(n)$ based on Eq. (2.50), with different colorcoding indicating the position of δg used in the left plot

higher-order corrections is therefore impossible.

We now want to consider the LHY-correction and see if we can find stable self-bound solutions. As a first heuristic approach, we compare the mean field energy according to Eq. (2.49) to the positive-definite three-dimensional LHY-correction in Eq. (2.25). The mean field energy needs to be negative definite to be able to form three-dimensional self-bound solutions. Continuing, we want to investigate this argument analytically. Starting by taking the sum of the energies and taking the negative derivative to the volume, gives the pressure.

$$P = -\frac{\partial}{\partial V} E_{tot}.$$

In a self-bound solution the pressure needs to vanish inside the droplet in order to create a force equilibrium. We continue for simplicity with $g_{11} = g_{22}$ and $n_1 = n_2$ as in general $g_{11}/g_{22} = n_1/n_2$:

$$\begin{aligned} E_{tot} &= E_{MF} + E_{LHY} \\ &= \frac{N^2}{2V}\left(\delta g + \frac{128}{15\sqrt{\pi}}(2gn)^{5/2}\right) \\ \Rightarrow P = -\frac{\partial}{\partial V} E_{tot} &= -\frac{1}{2}n^2\delta g - \frac{7}{4}\frac{128}{15\sqrt{\pi}} n^{9/2}(2g)^{5/2} \stackrel{!}{=} 0 \\ \Rightarrow \delta g &= -\frac{448}{15\sqrt{\pi}}(2gn)^{5/2}. \end{aligned} \tag{2.50}$$

The final result in Eq. (2.50) supports the prior heuristic approach and shows that droplet formation in three-dimensions only exists for negative mean field interaction. Fig. (2.2) shows

Eq. (2.50) while indicating the respective interaction energy $E_{MF} + E_{LHY}$ in Fig. (2.2a). For lower δg the negative bulge in energy becomes smaller, so that it is only possible to form self-bound systems for $\delta g < 0$. Further we recognise that, due to the pressure equilibrium independent of the local position, the density must form equi-density surfaces. In three-dimensions and in absence of any outer confinement or dynamics that could alter the shape, this will lead to a spherical density distribution.

Chapter 3 | Pseudo fourth- and second-order spectral algorithm to solve the GPe

We now want to turn towards describe an algorithm that solves the GPe in imaginary time, in order to find a stable ground state. In earlier years, the Crank-Nicholson method was used to solve the GPe and similar coupled partial differential equations. Only recently a change to spectral methods was made, methods that heavily rely on the fast Fourier transform. This thesis relies in particular on a pseudo-fourth- and second-order algorithm to solve the GPe in imaginary time, which was proposed and implemented many years ago [47, 48], so that this thesis does not present the development of such an algorithm, but displays a new utilisation in the coming results chapter. However, we use a modified algorithm, that solves the rotating GPe, exploiting the analogy between rotation and a particle in a magnetic field. Despite being able to change the algorithm to real-time propagation, imaginary time is preferred as only imaginary-time propagation offers a convergence to stable solutions, via the quantum mechanical time operator $\hat{\mathbf{U}}$ [49]

$$\hat{U} = e^{-\tau \hat{H}}. \tag{3.1}$$

First, we want to create a connection between the Hamiltonian for a charged particle in a magnetic field and a rotating Hamiltonian. This will prove useful later when we discuss the algorithm. Introducing the Hamiltonian for the charged particle in a magnetic field [50]:

$$\hat{H} = \frac{1}{2m}\left(\mathbf{p} + \frac{e}{c}\mathbf{A}\right) - e\Phi, \tag{3.2}$$

with $\mathbf{A}$ and Φ respectively the vector and scalar potential. We insert for the vector potential in two-dimension $\mathbf{A} = B(y\hat{e}_x - x\hat{e}_y)$ which gives

$$\hat{H} = \left(\mathbf{p}^2 + \mathbf{p}eB\left(y\hat{x} + x\hat{y}\right) + e^2B^2\frac{1}{4}\left(x^2 + y^2\right)\right) - e\Phi, \tag{3.3}$$

with $\mathbf{p}eB\left(y\hat{x} + x\hat{y}\right) = -i\hbar\nabla eB\left(y\hat{x} + x\hat{y}\right) = -i\hbar eB\boldsymbol{\nabla}\times\mathbf{r} = eBL_z$, where we see a connection to rotation for the first time, in the angular momentum L_z. Assuming $eB = \Omega$ gives

$$\left(-i\frac{\hbar^2}{2m}\boldsymbol{\nabla} - \Omega L_z + \frac{1}{4}\Omega^2 r^2\right) - e\Phi. \tag{3.4}$$

Repeating this for the Hamiltonian for rotation, which is given by [50]

$$\begin{aligned} H_\Omega &= H - \Omega L_z \text{ with } H = -i\frac{\hbar^2}{2m}\boldsymbol{\nabla} + V_{ext} \\ \Rightarrow H_\Omega &= -i\frac{\hbar^2}{2m}\boldsymbol{\nabla} + V_{ext} - \Omega L_z \end{aligned} \tag{3.5}$$

Comparing Eq. (3.5) to Eq. (3.4) we see that V_{ext} must be equal to $(1/4)\Omega^2 r^2$ to equalize Eq. (3.4) and Eq. (3.5). As we can change the external potential in any way possible in the previous algorithm without consequences, we subtract $(1/4)\Omega^2 r^2$ as a constant term of V_{ext} to transform the algorithm into the rotational case. Replacing B in the previously described algorithm with the rotational frequency Ω, allows for solving the GPe with external rotation.

After establishing this connection we derive the algorithm by discussing how to solve the one-dimensional harmonic oscillator, before solving the GPe and later with the correct substitutions using this to solve the charged particle in a magnetic field. The one-dimensional harmonic oscillator is given by:

$$\hat{H} = T + V = \frac{1}{2m}\hat{p}^2 + \frac{1}{2}m\omega^2\hat{x}^2. \tag{3.6}$$

One can write its density matrix (or imaginary time operator) as [49, 51]:

$$e^{-\tau(T+V)} = e^{-\tau C_V V} e^{-\tau C_T T} e^{-\tau C_V V} + \mathcal{O}(\tau^3), \tag{3.7}$$

where we will determine the functions C_V and C_T later on. One does this by evaluating Eq. (3.6) in Eq. (3.7)

$$\langle x'| e^{-\tau C_V V} e^{-\tau C_T T} e^{-\tau C_V V} |x\rangle = e^{-\tau C_V \omega^2 x'^2/2} e^{-(x'-x)^2/(2\tau C_T)} e^{-\tau C_V \omega^2 x^2/2}. \tag{3.8}$$

We know the exact expression of the density matrix for the left-hand side [37]

$$\begin{aligned}\langle x'| e^{-\tau(T+V)} |x\rangle &= \exp\left[-\frac{\omega}{2\sinh\omega\tau}\left(\left(x'^2 + x^2\right)\cosh\omega\tau - 2x'x\right)\right] \\ &= \exp\left[-\frac{\omega}{\omega\tau}\left(\left(x'^2 + x^2\right)\right)\left(\cosh\omega\tau - 1\right) + \left(x'^2 + x^2\right)^2\right)\right].\end{aligned} \tag{3.9}$$

with $-2x'x = (x'-x)^2 - x'^2 - x^2$. Comparing Eq. (3.8) and Eq. (3.9) for C_T and C_T gives

$$C_V = \frac{\cosh\omega\tau - 1}{\omega\tau\sinh\omega\tau} \text{ and } C_T = \frac{\sinh\omega\tau}{\omega\tau}. \tag{3.10}$$

Aiming for real-time propagation, one substitutes $\tau = it$, which gives

$$C_V = \frac{1 - \cos(\omega t)}{\omega t \sin(\omega t)} \text{ and } C_T = \frac{\sin(\omega t)}{\omega t}. \tag{3.11}$$

We then iterate the discretised wave function forward in imaginary time via

$$|\Psi(\tau + \Delta\tau)\rangle = e^{\Delta\tau(T+V)} |\Psi(\tau)\rangle. \tag{3.12}$$

The condensate ground state Ψ_0 can then be calculated for a particular set of input parameters:

$$\Psi_0 \approx \lim_{\tau\to\infty} \Psi(\tau) = \lim_{\tau\to\infty} e^{-\tau[T+V(\tau)]}\Psi(0), \tag{3.13}$$

where $\Psi(0)$ is our initial wavefunction at $\tau = 0$. Now that we know how to solve the one-dimensional harmonic oscillator via imaginary time-evolution, we apply the found expression to the GPe. We can rewrite the single-component GPe as [49, 51]

$$(T + V)\Psi(x, y) \text{ with } V = g|\Psi|^2. \tag{3.14}$$

Following imaginary time evolution, the condensates ground state is then given as Eq. (3.13)

$$\Psi_0 \approx \lim_{\tau\to\infty} \Psi(\tau) = \lim_{\tau\to\infty} e^{-\tau[T+V(\tau)]}\Psi(0).$$

Thus, we can solve the GPe the same way as a harmonic oscillator [49, 51].

While Eq. (3.7) describes a second order factorisation, we are interested in a fourth order algorithm. It can be shown that a fourth order algorithm is described by [49, 51]

$$T^{(4)}(\tau) = e^{-\frac{1}{6}\tau\hat{V}(\alpha)}e^{-\frac{1}{2}\tau}e^{-\frac{2}{3}\tau\tilde{V}(\alpha)}e^{-\frac{1}{2}\tau\hat{T}}e^{-\frac{1}{6}\tau\hat{V}(\alpha)}, \tag{3.15}$$

with $\hat{V}(\alpha) = V + \frac{\alpha}{48}\tau^2[V,[T,V]]$ and $\tilde{V}(\alpha) = V + \frac{1-\alpha}{24}\tau^2[V,[T,V]]$. Considering $\alpha = 1$ turns $\tilde{V} = V$.

Furthermore, we can use the algorithm to solve a harmonic oscillator by displaying a charged particle in a magnetic field as [51]

$$\begin{aligned} \hat{H} &= \frac{1}{2}\left(\Pi_x^2 + \Pi_y^2\right) \\ \text{with } \Pi_x = p_x - A_x &= -i\frac{\partial}{\partial x} + \frac{1}{2}By \;\; \Pi_y = p_y - A_y = -i\frac{\partial}{\partial y} + \frac{1}{2}Bx. \end{aligned} \tag{3.16}$$

Landau found that $[\Pi_x, \Pi_y] = iB$ which is analogous to $[\omega x, p_y] = i\omega$. We can identify the corresponding terms in the harmonic oscillator $P = \Pi_y$, $Q = \Pi_x/B$ and $\omega = B$. The operators are then $T = \Pi_y^2/2 = p^2/2$ and $V = \Pi_x^2/2 = \omega^2 Q^2/2$, respectively.

From Eq. (3.15) the fourth order algorithm for a charged particle in a magnetic field then goes as follows [51]:

1. Start with a suitable set of initial conditions that allows for finding the ground state
2. Multiply ψ with $\exp\{-\tau V/6\}$, where V is the external potential
3. Compute the Fourier transform from $\psi(x, y)$ to $\psi(p_x, y)$ and multiply by $\exp\{-\tau C_V(1/4)(p_x + By)^2\}$
4. Compute the Fourier transform from $\psi(p_x, y)$ to $\psi(x, p_y)$ and multiply by $\exp\{-\tau C_T(1/4)(p_y + Bx)^2\}$
5. Compute the Fourier transform from $\psi(x, p_y)$ to $\psi(p_x, y)$ and multiply by $\exp\{-\tau C_V(1/4)(p_x + By)^2\}$

At this point we encounter the $(1/48)\tau^2[V,[T,V]]$ term in Eq. (3.15), the effective midpoint potential where

$$[V,[T,V]] = \left(\frac{\partial V}{\partial x}\right)^2 + \left(\frac{\partial V}{\partial y}\right)^2. \tag{3.17}$$

The algorithm continues as follows

6. calculate positional derivatives of the effective potential and multiply by $\exp\left\{-\tau(2/3)\left(V\tau^2/48\left(\mathrm{Re}\left(\frac{\partial V}{\partial x}\right)^2 + \mathrm{Re}\left(\frac{\partial V}{\partial y}\right)^2\right)\right)\right\}$
7. Compute the Fourier transform from $\psi(x,y)$ to $\psi(p_x,y)$ and multiply by $\exp\{-\tau C_V(1/4)(p_x+By)^2\}$
8. Compute the Fourier transform from $\psi(p_x,y)$ to $\psi(x,p_y)$ and multiply by $\exp\{-\tau C_T(1/4)(p_y+Bx)^2\}$
9. Compute the Fourier transform from $\psi(x,p_y)$ to $\psi(p_x,y)$ and multiply by $\exp\{-\tau C_V(1/4)(p_x+By)^2\}$
10. Transform back to $\psi(x,y)$ and multiply by $\exp\{-\tau V/6\}$
11. Normalise the resulting wavefunction and repeat from step 1 until convergence is reached.

Thus, we can solve the GPe by making the right substitutions and display it as a charged particle in a magnetic field.

During the time working on this thesis we switched from the previously described pseudo fourth-order algorithm to a second-order algorithm. The algorithm in itself as described in the aforementioned numerated list stays mostly the same, only changing the imaginary time propagation operator to

$$T^{(2)}(\tau) = e^{-\frac{1}{2}\tau V(\tau)} e^{-\tau} e^{-\frac{1}{2}\tau V(0)} \tag{3.18}$$

and thus reducing the steps to the respective amount in the operator. The change was done due to a switch from a single-processor CPU code to a parallelised GPU-code, offering a speed-up by approximately 10^5, thereby allowing for the numerical results in the following chapters.

Chapter 4 | Lower dimensionality in BEC

The previously discussed systems were exclusively three-dimensional. However, our interest lies in lower-dimensional systems, particularly two and quasi-two-dimensions, as they offer easier computational accessibility. While the general physics in lower-dimensional systems remains the same, the interaction density's mathematical expression changes. In this chapter we will discuss those changes, starting with creating a framework that allows us to differentiate between the different dimensional states. Further, we will transform the mean field and LHY-energy into their lower-dimensional expressions.

We introduce the minimum excitation energy ϵ_0

$$\epsilon_0 = \frac{\hbar^2}{2m}\left(\frac{2\pi}{a_z}\right)^2, \tag{4.1}$$

where a_z is the length scale of external confinement, that squeezes the system into lower dimensionality with ϵ_0 in the confined direction. A given system is lower-dimensional when neither thermal fluctuations nor the interaction energy are large enough to allow excitation in the confined direction, i.e. $g_{11}n_1 + g_{22}n_2 \ll \epsilon_0$ and $k_BT \ll \epsilon_0$. As we are dealing with perfect conditions for condensation, $k_BT \ll \epsilon_0$ is always fulfilled. Moreover, $g_{11}n_1 + g_{22}n_2 \ll \epsilon_0$ and $k_BT \ll \epsilon_0$ form an upper bound for the two-dimensional system. However, for a quasi-two-dimensional system, excitations in the confined direction are allowed, such that $g_{11}n_1 + g_{22}n_2 > \epsilon_0$ and thus $a_z > a_s$ and $a_z \ll L_{x,y}$, so that the condensate geometrically speaking looks two-dimensional [35].

The mean field energy in three-dimensions is given by $E = gn^2/2$ with the particle density $n = |\Psi(\mathbf{r}, t)|^2$. We reduce the mean field interaction energy by following a local density approximation, which allows for assuming that the Hamiltonian of the system is separable in the z-direction. Thus, the wavefunction is

$$\psi(x, y, z) = \Phi(x, y) \times Z(z). \tag{4.2}$$

We will squeeze the condensate in z-direction via a harmonic trap. In the mean field description of the ground state energy, the particles linear momentum $\mathbf{p}$ equals zero. Thus the condensate will find itself in the ground state so that $Z(z)$ takes the shape of a Gaussian

$$Z(z) = \frac{1}{\pi^{1/4}a_z^{1/2}}e^{-\frac{z^2}{2a_z^2}}.$$

The square of the particle density n is then

$$n^2 = |\Phi(x, y)|^4|Z(z)|^4 = n_{Q2D}^2|Z(z)|^4,$$

and inserting $Z(z)$ into this, gives

$$|Z(z)|^4 = \sqrt{\left(Z(z)Z^*(z)\right)^4} = \left(\pi^{1/2}a_z\right)^{-2} e^{-\frac{2z^2}{a_z^2}}. \tag{4.3}$$

We integrate this over the whole space in z-direction,

$$\int_{-\infty}^{\infty} |Z(z)|^4 \, dz = \left(\pi^{1/2}a_z\right)^{-2} \int_{-\infty}^{\infty} e^{-\frac{2z^2}{a_z^2}} \, dz = \frac{1}{\sqrt{2\pi}a_z}, \tag{4.4}$$

which gives for the mean field energy

$$E = \frac{g n_{Q2D}^2}{\sqrt{2\pi}} a_z. \tag{4.5}$$

Petrov derived a more general expression for both, the exact two-dimensional and quasi-two-dimensional case [52]:

$$g = \frac{2\sqrt{2\pi}\hbar^2}{m} \frac{1}{a_z/a_s + (1/\sqrt{2\pi}\ln(1/\pi q^2 a_z^2))}. \tag{4.6}$$

We now further introduce the limitation that $a_z \gg a_s$, with a_s being the three-dimensional s-wave scattering length, which needs to be fulfilled for having a quasi two-dimensional system. This is equivalent to $g_{11}n_1 + g_{22}n2 \ll \epsilon_0$. For $a_z \gg a_s$ the zeroth-order mean field interaction energy becomes equal to Eq. (4.5) when exchanging g with Eq. (4.6).

As previously mentioned, Eq. (2.25) given for the three-dimensional LHY energy in Ch. 2.3, only adheres to free space. Even if one goes one step back and repeats the integration with the above local density approximation, one gets an erroneous result, as the energy values in the z-direction are assumed to be continuous. Thus we need a more general expression, which is given in the original paper by Lee, Huang and Yang, and also by Zin [28, 35],

$$\frac{\epsilon_0}{L^3} E_{LHY} = \lim_{r\to 0} \frac{\partial}{\partial r} \left(r \frac{1}{2V} \sum_k e^{ikr} \left(\epsilon_k - A_k\right) \right) \quad \text{for} \quad g_{12} = -\sqrt{g_{11}g_{22}}. \tag{4.7}$$

Here L is the size of a box potential, $\epsilon_0 = \hbar^2/2m\,(2\pi/L)^2$ the minimal excitation energy, $\epsilon_k = \sqrt{E_k^2 + 2E_k(g_{11}n_{11} + g_{22}n_{22})}$, $A_k = E_k + g_{11}n_{11} + g_{22}n_{22}$ and $E_k = \hbar^2k^2/2m$ [35]. The prefactor ϵ_0/L^3 has been extracted to make Eq. (4.7) dimensionless and should be restored when using E_{LHY} in simulations. In three-dimensions we would now change the sum over k-space into a phase space integral and would yield prior three-dimensional results in Eq. (2.27). For quasi-two-dimensions we still integrate over the two unconfined directions, while keeping the sum for the confined one,

$$\frac{1}{V}\sum_k \to \frac{1}{(2\pi)^2} \int d^2k_\perp \frac{1}{L} \sum_{k_z},$$

so that

$$E_{Q2D,LHY} = \lim_{r\to 0} \frac{\partial}{\partial r} \left(r \frac{1}{2} \sum_{q_z} \int d^2q_\perp e^{iqr} (\epsilon_q - A_q) \right), \tag{4.8}$$

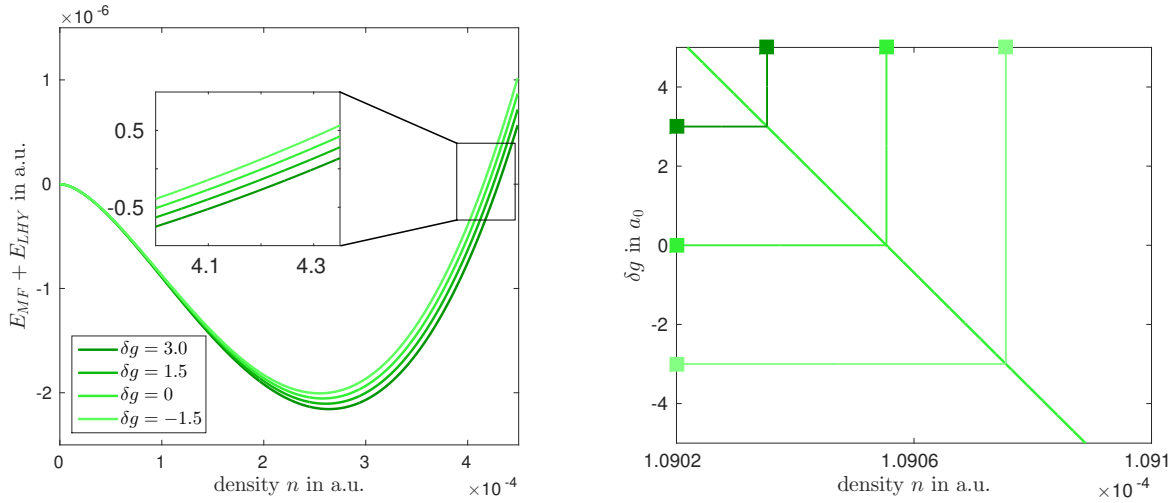

Figure 4.1: Left: $E_{MF} + E_{LHY}$ for different δg in the range from 3.0 to -1.5, based on Eq. (4.9). The energies have similar shapes for all values of δg, so that stable solutions are possible for repulsive and attractive mean field interaction
Right: $\delta g(n)$ based on Eq. (5.1), with different colorcoding indicating the position of δg used in the plot to the left

with $q_i = L/(2\pi)k_i$, $\epsilon_q = \sqrt{q^4 + 2\xi q^2}$, $A_q = q^2 + \xi$ and $\xi = (g_{11}n_{11} + g_{22}n_{22})/\epsilon_0$. Further calculation gives, that Eq. (4.8) approximates to [35]

$$E_{LHY}(\xi) = \frac{\pi}{4}\xi^2 \left(\log(\xi) + \log\left(2\pi^2\right) + \frac{1}{2} + \frac{\pi^2 \xi}{3} \right), \tag{4.9}$$

for $\xi < 0.3$, while for $\xi \geq 0.3$ Eq. (4.8) equals the three-dimensional two-component interaction Eq. (2.27). So that Eq. (4.9) is only valid for very dilute parts of the gas with small ξ or for small trap sizes with high minimal excitation energy ϵ_0. We see that Eq. (4.9) is not positive-definite, resulting in an attractive LHY-term compared to the purely repulsive term in the three-dimensional case. This will be particularly interesting for the formation of self-bound droplets.

Additionally, we can derive the exact two-dimensional LHY-energy by inserting the two-dimensional scattering length in the expressions given by Petrov for two-dimensional energy and condensate density, where the two-dimensional scattering length is given by [35, 53]:

$$a_{2d} = 2L e^{-\gamma - \frac{L}{2a_{3d}}}. \tag{4.10}$$

The energy E_{2d} and condensate density n_0, for symmetric components, is obtained by: [53]

$$\begin{aligned} n_0 &= \frac{\exp\left(-2\gamma - \frac{3}{2}\right)}{2\pi} \frac{\ln\left(\frac{a_{12,2d}}{a_{2d}}\right)}{a_{2d} a_{12,2d}}, \\ E_{2d} &= \frac{8\pi n^2}{\ln^2\left(\frac{a_{12,2d}}{a_{2d}}\right)} \left[\ln\left(\frac{n}{n_0}\right) - 1 \right], \end{aligned} \tag{4.11}$$

which gives Eq. (4.9) with the last term omitted.

Chapter 5 | Results

In the previous chapters we started by describing BECs and their energetic properties in and beyond mean field as well as their rotational dynamics. Followed by the dimensional reduction to quasi-two- and two-dimensions, we established the numerical algorithm used to solve the rotational GPe , so that the adaptation of the algorithm is original in this thesis. In the following chapter, we present the obtained results in a quasi-two-dimensional system and compare them to the previous chapters and the current literature. Starting with droplet formation in the given system and the rotational dynamics of a trapped LHY-fluid, we merge both sections by studying the real-time dynamics of vortices in self-bound quasi-two-dimensional droplets via extended mean field theory.

5.1 Formation of droplets in lower dimensions

In Ch. 4, we gave the LHY energy for a quasi-two-dimensional system, which can be negative compared to the positive-definite three-dimensional LHY-correction. As discussed, this leads to a higher number of self-bound solutions across a wider range of parameters with respect to δg as indicated by Fig. (4.1, left). We now want to investigate the droplet formation and shape for such systems, by first deriving the pressure equilibrium and then making an educated guess on the resulting equation. The chapter finishes by showing example systems for various physical parameters based on simulations via the algorithm described in Ch. 3.

We calculate the pressure in the given system by taking the derivative of the energy with respect to the volume inhabited by the condensate. Enforcing equal pressure throughout the droplet, this yields an expression for the existence of droplets in a certain range of parameters [35]. The energy for a quasi-two-dimensional system in mean field with LHY-correction is given by

$$\begin{aligned} E_{tot} &= E_{MF} + E_{LHY} \\ &= \frac{N^2}{2V}\delta g + \frac{\epsilon_0}{L^3} V \frac{\pi}{4} \left(2g\frac{N}{V\epsilon_0}\right)^2 \left(\log\left(\frac{2gn}{\epsilon_0}\right) + \log\left(2\pi^2\right) + \frac{1}{2} + \frac{\pi^2(2gn)}{3\epsilon_0}\right). \end{aligned}$$

Taking the derivative to the volume gives us the pressure P,

$$\begin{aligned} \Rightarrow P &= -\frac{\partial}{\partial V} E_{tot} = -\left(E_{MF} + E_{LHY,Q2D} + \frac{\epsilon_0}{L^3}\frac{\pi}{4}\left(\frac{2gn}{\epsilon_0}\right)^2\right) \stackrel{!}{=} 0 \\ \Rightarrow \delta g &= -2\pi g^2 \left[\log\left(\frac{2gn}{\epsilon_0}\right) + \log\left(2\pi^2\right) + \frac{3}{2} + \frac{\pi^2 2gn}{3\epsilon_0}\right] \frac{\epsilon_0}{L^3}, \end{aligned} \tag{5.1}$$

with all parameters as before. We plot Eq. (5.1) in Fig. (4.1, right) and see behavior similar to Fig. (4.1, left). In Fig. (4.1, left) and Fig. (4.1, right) the solution's distance in particle density

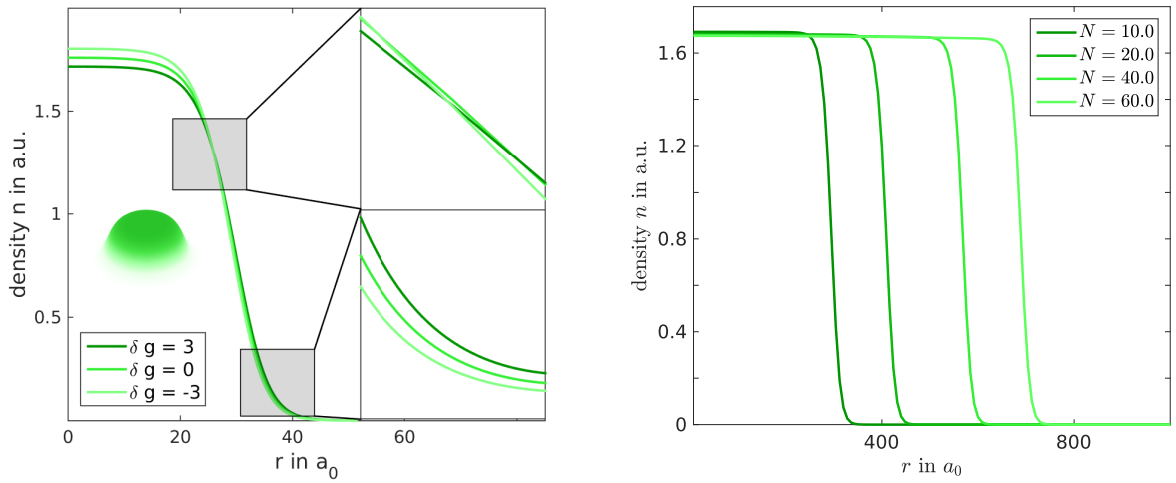

Figure 5.1: Left: Radial density distribution of quasi-2-dimensional self-bound systems for $g = 50$ and δg in the range displayed. We find that for higher δg the steepness of fringes decreases. Additionally, we see that, despite the symmetrical distribution around $\delta g = 0$, the other two do not intersect $\delta g = 0$ symmetrically in the top right panel.
Right: Radial density distribution of quasi-2-dimensional self-bound systems for $g = 50$, $\delta g = 0$ and the norm fixed to the display values. With increasing norm, the droplet only increases in size, but not its particle density n. This confirms our result in Eq. (5.1).

n is small. Based on that observation, we can assume to find stable self-bound droplet solutions for a wider range of parameters δg, that would be inaccessible for the three-dimensional case. Due to the dependence on the particle density n in Eq. (5.1) and the restrictions towards a pressure equilibrium, we expect a flat-top density distribution with a steep descent towards the edges. Furthermore, an increase in particles N should not alter the particle density of a stable solution, but only increase the width of the droplet.

We want to confirm the above heuristic approach by solving the system numerically. We start by taking the derivative of $E_{LHY,Q2D}$ to the density in order to yield a potential that we can feed into the GPe

$$V_{LHY,Q2D} = \frac{\partial}{\partial n} E_{Q2D,LHY} = \frac{\pi}{\epsilon_0^2} g\xi \left(\log(\xi) + 1 + \log\left(2\pi^2\right) + \frac{\pi^2}{2}\xi \right) \frac{\epsilon_0}{\sqrt{8}\pi^3}, \tag{5.2}$$

with all the parameters as before. We propagate Eq. (2.9) using the algorithm described in Ch. 3 with $V_{ext} = V_{LHY,Q2D} + V_{MF}$ and $\omega = \Omega = 0$. First we are interested in the shape of the droplet, where we find three different solutions with a fixed norm $N = 1$, $g_{11} = g_{22}$ and $\delta g = g_{12} + \sqrt{g_{11} g_{22}} = [-3.0, 0.0, 3.0]$ so that $\delta g \ll g_{11} = g_{22}$. The density distribution is shown in Fig. (5.1, left). We find similar shapes for all three configurations, only differing in height and steepness at the fringes of the distribution. For smaller δg the height and steepness increases, as indicated by the main plot and the bottom right subplot. $\delta g = 3.0$ and $\delta g = -3.0$ have different crossing points with $\delta g = 0.0$ despite symmetrical distribution of g. This comes from the nonlinearity of $V_{LHY,Q2D}$. Additionally, we plotted the density distribution as a surface plot as little inlay within the plot for $\delta g = 0.0$.

We are also interested in how the droplet shape changes with increasing particle number N. By increasing N to $N = [10, 20, 40, 60]$ in Fig. (5.1, right), we confirm the assumptions made in the heuristic approach, that the density for a stable solution stays unaffected by the particle number and only changes the extent of the droplet.

5.2 Rotational dynamics of a trapped LHY-fluid

As we saw in Sec. 2.4 the shape and form of interaction of a condensate influences the rotational dynamics of the condensate. We now want to investigate how its dynamical behaviour changes for a trapped system governed by quantum fluctuations that without the trap would form a stable droplet. Starting off by revisiting the continuity equation Eq. (2.28) and energy expectation value Eq. (2.38) we then chose the same system as in Ch. 2.4 for Fig. (2.1) but choose $\delta g = 0.0$, so that the LHY contribution is the only effective particle-particle interaction of the system.

We remember that the continuity equation comes from multiplying Eq. (2.9) with Ψ_0^* and subtracting the complex conjugation of the result from itself. Because of this, only imaginary parts of the equation survive, making the continuity equation independent of any real V_{ext}. Henceforth, we obtain the same quantised-irrotational dynamics and vortex formation as described in Ch. 2.4.

The energy of a uniform medium governed by quantum fluctuations with a vortex of rotational quantisation l in cylindrical coordinates is then similarly to Eq. (2.38) given by

$$E = \int d\,\mathbf{r} \left[\frac{\hbar}{2m} |\boldsymbol{\nabla} \Psi_0(\mathbf{r})|^2 + \frac{\pi}{4} \left(\frac{U_0}{\epsilon_0} |\Psi_0(\mathbf{r})|^2 \right)^2 \cdot \right.$$
$$\left. \cdot \left(\log \left(|\Psi_0(\mathbf{r})|^2 \frac{U_0}{\epsilon_0} \right) + 0.5 + \log\left(2\pi^2\right) + \frac{\pi^2 U_0 |\Psi_0(\mathbf{r})|^2}{3\epsilon_0} \right) \frac{\epsilon_0}{\sqrt{8}\pi^3} \right]. \tag{5.3}$$

As done in Sec. 2.4 this can be used to calculate the energy and critical angular momentum for vortex creation or to study multiple off-axis vortices as done in [44, 54, 55]. However, this is not in scope of this thesis.

To offer a quantitative description of the differences in rotational dynamics between mean field and LHY-correction, we plot $L(\Omega)$ with the same parameters as in Fig. (5.2). The LHY dominated condensate shows, as expected, the same quantised increase in angular momentum as pure mean field interaction in Fig. (2.1). However, the critical angular momentum for the symmetry breaking by introducing an additional vortex to the system is drastically lowered for LHY. This is as expected as the LHY-correction is generally much weaker than the mean field interaction. In the mean field, a weaker interaction should come with a larger vortex core, which is the opposite of what we see for the LHY-fluid. Additionally, the $L(\Omega)$ slope for a higher number of vortices is smaller for LHY and the system's angular momentum for higher vortex states increases compared to mean field. The slope corresponds to the

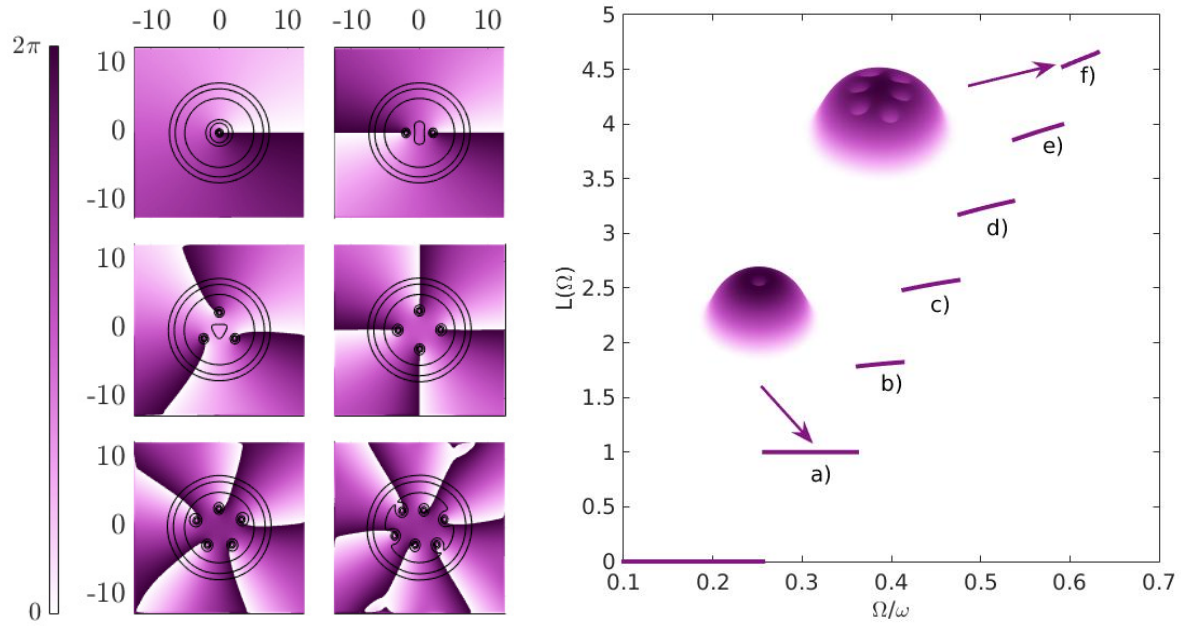

Figure 5.2: Left: Vortex density distributions as indicated by the labels. For vortex numbers $l > 5$ we find a different distribution of vortex positions within the condensate, as for a purely mean field interacting Bose gas.
Right: $L(\Omega/\omega)$ for LHY-interaction $g = 50$ and $\omega = 0.1$. We see the existence of critical external rotation Ω_c, which leads to a phase-transition between states of higher vorticity. However, due to the weaker LHY-correction compared to mean field, the critical angular momentum is lower.

movement of vortices to the centre of the condensate, thus increasing angular momentum per particle. Furthermore, the $L(\Omega)$ and Ω/ω spacing between different symmetries seem to be more equal. All of this shows that there is still much to understand and invites for a expanding study of the system similar to [44, 54, 55]. For a easier comparison, both Fig. (2.1) and Fig. (5.2) are given again in App. (B).

5.3 Real-time dynamics of rotating self-bound quasi-two-dimensional droplets

Understanding the droplet formation and rotational dynamics of quasi-two-dimensional Bose-gases governed to a large extent by quantum fluctuations, we now want to investigate the real-time dynamics of rotating droplets. This poses an interesting question, as a droplet is in a pressure equilibrium, sensitive to any perturbation. Thus it is not trivial whether a centrifugal force due to rotation breaks that equilibrium.

We focus on real-time stability and dynamics. From a classical point of view, a rotating harmonic oscillator is stable as long as $\Omega \leq \omega$. A self-bound droplet, however, requires $\omega = 0.0$, so that we cannot rotate a self-bound droplet without it leaving pressure equilibrium. It is worth noting that the mean field energy, as well as the LHY-correction, can

act as a confining energy, thus giving some margin for rotation $\Omega > \omega$. For mean field this margin was calculated by Rosenbusch *et al.* in [56], but has yet to be calculated for the LHY-correction of any dimensionality. Additionally, in recent publications, either a wavefunction with vorticity according to Eq. (2.34) was assumed as a solution of the GPe [57], or it was a study about real-time stability of those phase-inprinted states [58]. In the following sections, we will find a ground state with m vortices via imaginary time propagation, then release the system by decreasing the harmonic trap linearly

$$\omega(t) = \begin{cases} \omega_0 - vt & \text{if } vt < \omega_0 \\ 0 & \text{if } vt \geq \omega_0 \end{cases} \tag{5.4}$$

and turning off the external rotation Ω completely. After the full trap release, i.e. $\omega(t) = 0$ we study the real-time stability and dynamics for a unit vortex and multiple single-quantised vortices.

5.3.1 Unit vortex

We start off by investigating the unit vortex, as it is the easiest system to analyse, but still provides interesting physics as we will see. Initially we create a number of converged trapped BECs with a unit vortex. We choose $g = 50$, $N = 15$, $\delta g = 0$, $L = \sqrt{8\pi}$ and $\omega_0 = 0.0025$. All of the parameters are chosen heuristically, however, ω_0 is chosen small enough, so that the shape is not dominated by the Gaussian as seen in the density inlay in Fig. (5.3, right).

The angular momentum $\langle L_z \rangle$ is conserved in real time as we show in App. (D). We can then use $\langle L_z \rangle$ as an important benchmark, as deviations can then only occur due to numerical truncation errors or non-physical behaviour of the system.

Initially, the behaviour for different trap opening speeds during the opening sequence is of interest. For three different sets of condensates, we open the trap with speeds $v = [10^{-4}\omega_0, 10^{-3}\omega_0, 5 \cdot 10^{-3}\omega_0]$ and measure the maximum density in time, as well as the angular momentum. The results are displayed in Fig. (5.3) with the percentage of trap opening shown along the x-axis instead of time. We see that over the whole propagation time angular momentum is conserved. Moreover, for high opening rates the density oscillates on a negative slope, while for adiabatic opening speeds the density follows a steady Gaussian slope. In Fig. (5.3, left) the plotted density distributions are normalised to the maximum density value of the first column. As the trap releases the condensate, the density decreases, while the condensate and vortex core size grows. The rows correspond, from top to bottom, to $v = [10^{-4}\omega_0, 5 \cdot 10^{-3}\omega_0, 10^{-3}\omega_0]$. Despite the full shut-off of the trap, the condensate has not yet fully expanded for $v = 10^{-4}\omega_0$ at the end of the sequence. In the following we will study the difference between both cases after release. Due to the steady decrease in particle density n, we will choose $v \leq 10^{-4}\omega_0$ for following systems.

In Fig. (5.4) we show the time-evolution of a unit vortex directly after full release for $v = 10^{-3}\omega_0$. Due to the expansion velocity and the density dependence of the LHY-correction, the droplet slowly splits into two rings. These rings grow in radius and oscillate in size and

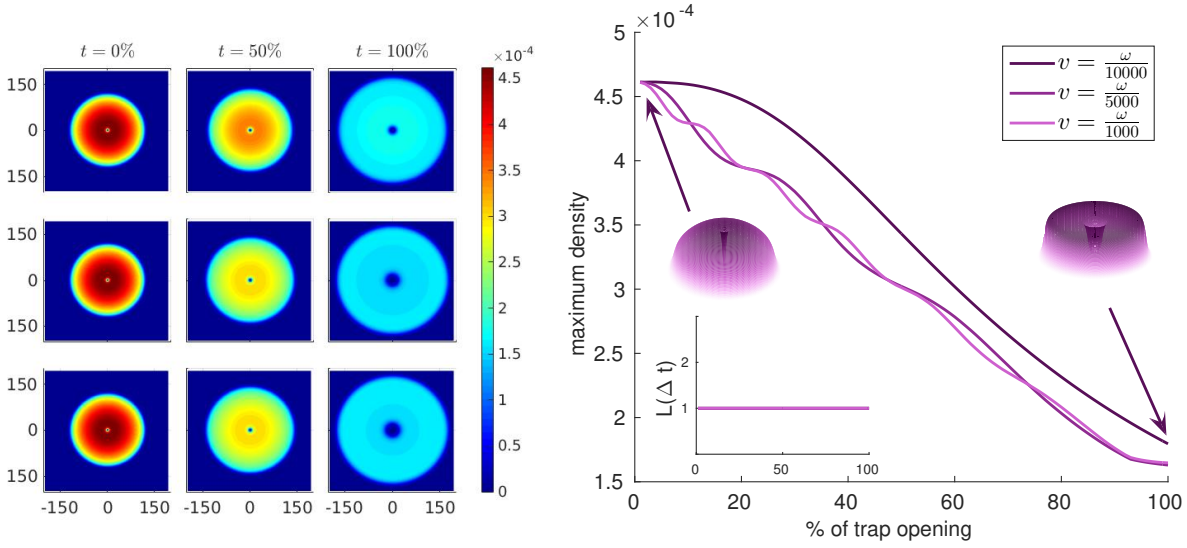

Figure 5.3: Left: Density distributions for all three systems at $g = 50$, $\omega_0 = 0.025$ and 0%, 50%, 100% trap opening. The density is given by red, the highest and blue, the lowest. Systems parameters as given in the text and opening speed from top to bottom $v = [10^{-4}\omega_0, 5 \cdot 10^{-3}\omega_0, 10^{-3}\omega_0]$
Right: Time evolution of the maximum density for each system, distinguished by the trap opening speeds as given in the plot. The surface plot corresponds to $v = 10^{-4}\omega_0$. Furthermore, we see that the angular momentum per particle is conserved.

density but never reconnect during the time evolution. They keep growing until the border of the mesh is reached. However, only investigating the real-time evolution holds no information about the systems physicality. As we established angular momentum as an important benchmark, we plot $\Delta L(t)/L_0$ in Fig. (5.5) for all v in a range $\Delta L(t)/L_0 \in [-0.01, 0.01]$ for times after full release from the harmonic oscillator. We see that for $v < 10^{-4}$ L deviates over time, thus, Fig. (5.4) shows an unphysical system. We call a system unphysical, when the set of chosen parameters Comparing the phase in Fig. (5.4) with Fig. (5.5, left) we find that the instability in the system is occurring at approximately the same time as a discontinuity in the phase shows.

Releasing the condensate adiabatically with $v \leq 10^{-4}\omega_0$ for $\omega_0 = 0.0025$ creates meta-stable solutions, that remain constant in their size and density over time. We define them as meta-stable, as they stay stable up to a certain point where numerical deviations lead to unstability of the system. Thus, we are uncertain about their permanent physical stability. Besides numerical deviations over time, we do not find any physical instabilities occurring. However, the radius of those meta-stable solutions changes periodically over time, depending on v, similar to the breathing mode in [39]. In Fig. (5.6, right) we plot the FWHM of the vortex core (bottom) and droplet size (top) for $\omega_0 = 0.0025$ and $v = [10^{-4}\omega_0, 2 \cdot 10^{-4}\omega_0]$. For both systems we see perdiodical changes in distance over time, which can be brought back to the particular density dependence of $V_{LHY,Q2D}$ and the expansion speed of the harmonic oscillator, which affects the vortex core size while opening the trap. Furthermore, for $v = 10^{-4}\omega_0$ we see a second small oscillation occurring for the vortex core size at its minima,

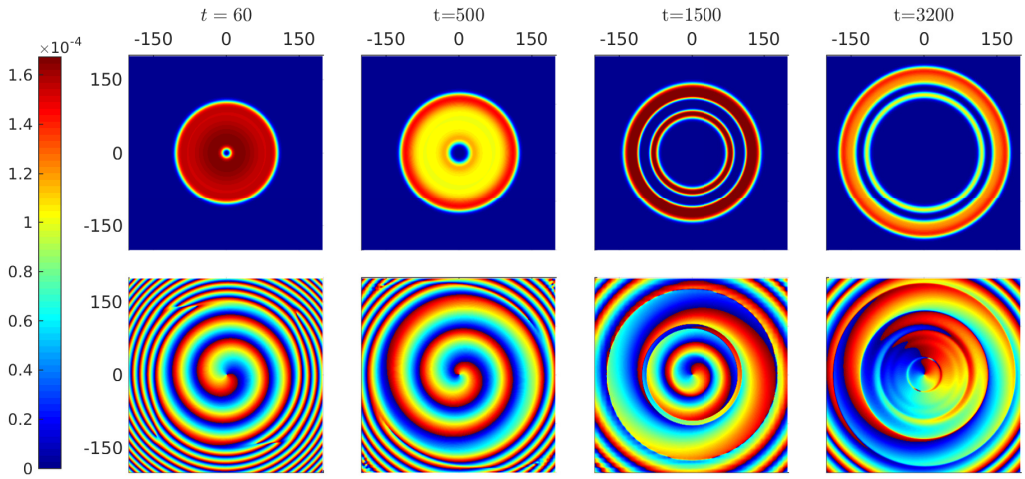

Figure 5.4: Time evolution of a unit vortex directly after full release with $v = 10^{-3}\omega_0$. Due to the velocity and the density dependence of the LHY-correction, two rings form, that expand as time continues, until they reach the border of the mesh. The density is normalised to the highest value at $t = 60$. The plot in the bottom shows the respective phase for each given density distribution.

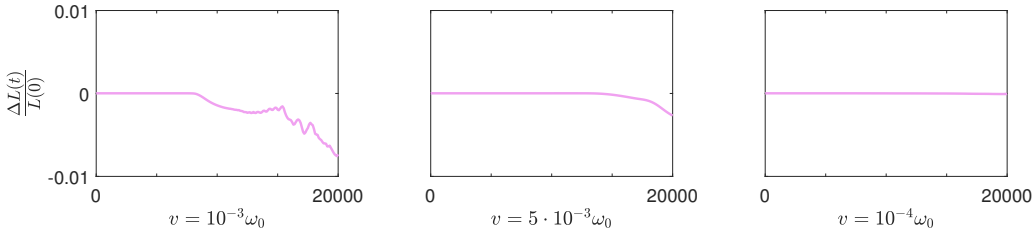

Figure 5.5: Deviation of angular momentum directly after full release from the trap for values of v as given in the plot. We see that for the studied system of propagating rings the GPe breaks down and thus yields unphysical results due angular momentum not being conserved.

originating from a density wave traversing through the droplet radially from the vortex core off phase with the main breathing mode. This can be seen in Fig. (5.6, left) for $v = 10^{-4}\omega$ and $t = 5950$ and more clearly in [59]. Fig. (5.6, left) shows the density distributions for $\omega_0 = 0.0025$ and $v = [10^{-4}\omega_0, 2 \cdot 10^{-4}\omega_0, 5 \cdot 10^4\omega_0]$ at same time differences, corresponding to Fig. (5.6, right). Both plots in Fig. (5.6) show the different oscillations frequencies and amplitudes for all systems, as well as the virtually undetectable breathing mode for $v = 5 \cdot 10^4\omega_0$.

5.3.2 Multiple vortices

We continue by increasing the number of vortices in the system and release the condensate adiabatically. With increasing number of vortices m, we also need to increase the particle number N, so that for $m = [1, 2, 3, 4]$ we use $N = [10, 15, 20, 30]$ respectively. For the trap opening speed we choose a value that resulted in stable systems for the unit vortex, i.e. $v \leq 10^{-4}$.

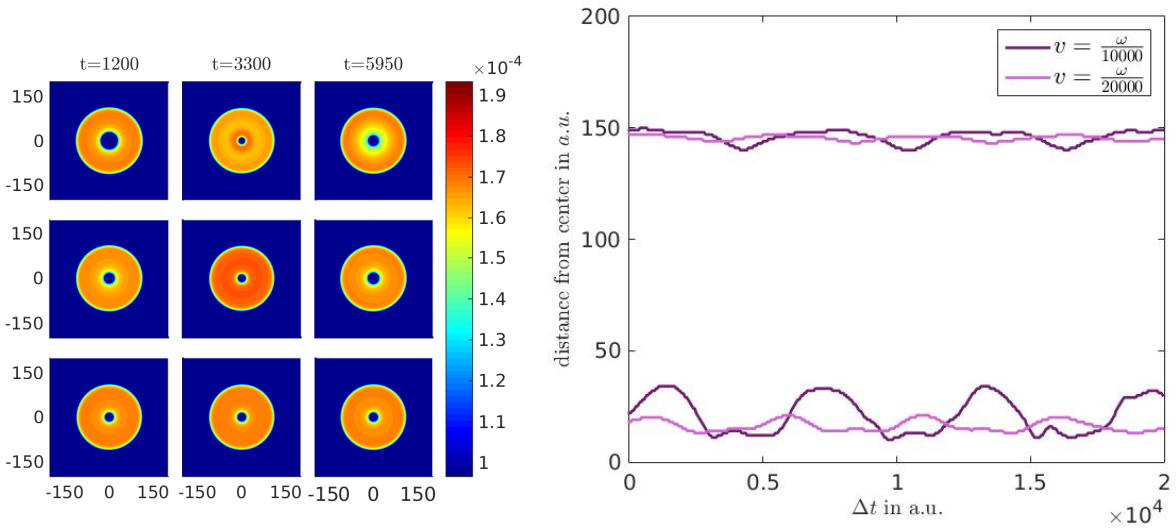

Figure 5.6: Left: Density distributions for three different trap opening speeds at different timesteps, whereas red is the highest and blue the lowest. From top to bottom: $10^{-4}\omega_0\,, 2\cdot 10^{-4}\omega_0\,, 5\cdot 10^{-4}\omega_0$
Right: time evolution of the full width half maximum of the droplet radius (top) and vortex core (bottom) for $10^{-4}\omega_0$ and $2\cdot 10^{-4}\omega_0$. We omitted $5\cdot 10^{-4}\omega_0$ to enhance clarity, due to a lack of variation, as indicated by the respective density distributions on the left.

Again, for all following number of vortices we investigate the real-time stability for the two trapsizes $\omega_0 = [0.0025, 0.001]$ and three opening speeds $v = [10^{-4}\omega_0, 2\cdot 10^{-4}\omega_0, 5\cdot 10^{-4}\omega_0]$ from Sec. 5.3.1 with $dt = 0.01$ per iteration. The stability of the system was found to be independent of dt within the validity of the second-order algorithm. Additionally, we provide a quantitative description of the rotational dynamics for a stable three-vortex system.

In Fig. (5.7) we plot the angular momentum expectation value $\langle L_z\rangle$ for all unit vortex systems discussed so far, and additionally for vortex numbers $m = [1, 2, 3, 4]$. $\langle L_z\rangle$ is normalised by $L(0)$ at the beginning of the trap opening. The light-purple systems represent $\omega_0 = 0.0025$ and the dark-purple $\omega_0 = 0.001$, while each row and column show systems as given in the labels in the plot. As angular momentum is supposed to be conserved (App. (D)) for any rotational symmetry, we recognise that all systems below the green line in Fig. (5.7) are unphysical due to their deviation. Thus, a higher number of vortices m requires a slower trap opening v or weaker initial trap ω_0. There are two different instabilities occurring. One where the system becomes unphysical over time, as in $m = 3$, $v = 10^{-4}\omega_0$. The other one, where the system starts with a deviation from $\Delta L(t)/L(0) = 0$ as in $m = 4$, $v = 5\cdot 10^{-4}\omega_0$. The latter is due to a deviation that occurs during the release process and can most likely be avoided with a more realistic non-linear opening procedure.

In the following, we describe the real-time evolution for droplets with multiple single quantised vortices, on the example of $m = 3$, $v = 10^{-4}\omega_0$ with $\omega_0 = 0.001$ according to Fig. (5.8). However, the same description can be applied to every other previously displayed system. Real-time evolutions for all systems as movies can be found at [59]. Furthermore, the de-

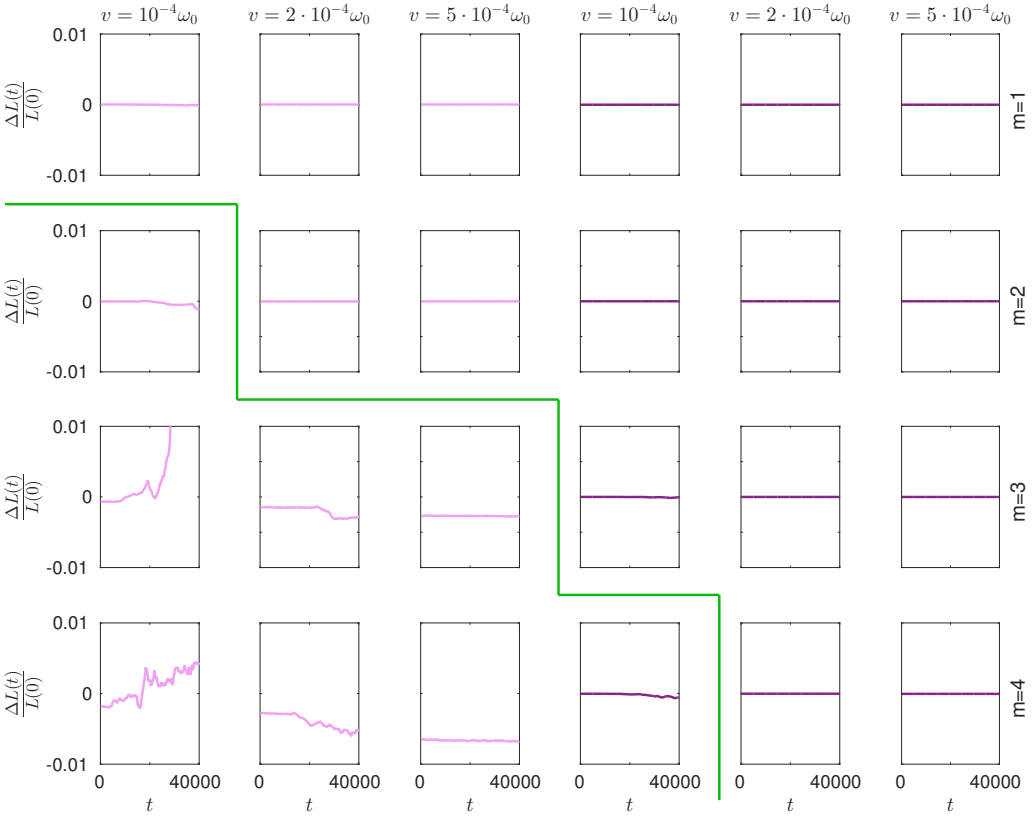

Figure 5.7: $\Delta L(t)/L(0)$ for $\omega_0 = 0.0025$ in light-purple and $\omega_0 = 0.001$ in dark-purple. Each column represents v and each row the number of vortices m as given in the figure. All systems below the green line are considered to be parameters where the GPe breaks down and produces unphysical results due to angular momentum conservation.

scription also fits the dynamics of two-dimensional systems, according to Eq. (4.11), as found in [60].

There are three features to observe, the first being the same breathing behaviour as observed for $m = 1$, where the breathing amplitude and frequency decrease as the opening speed decreases. Just as with the unit vortex, we see density waves traversing radially from each vortex core. Those waves reflect off the boundaries of the droplet in m-fold rotational symmetry. This leads to local asymmetric deviations of the particle density n around the vortex core and thus changes the healing length ξ asymmetrically around the vortex core. In Sec. 2.4 we established that for small rotation the vortex core size is approximately the healing length ξ, where $\xi = 1/\sqrt{2nU_0}$. As the density changes, so does ξ and thus the vortex cores obtain their irregular shape. With decreasing v this occurrence vanishes, as the resulting density waves amplitude decrease as well. The last feature to observe is that given enough time, the droplet obtains m-fold rotational symmetry, where m is the number of vortices as before.

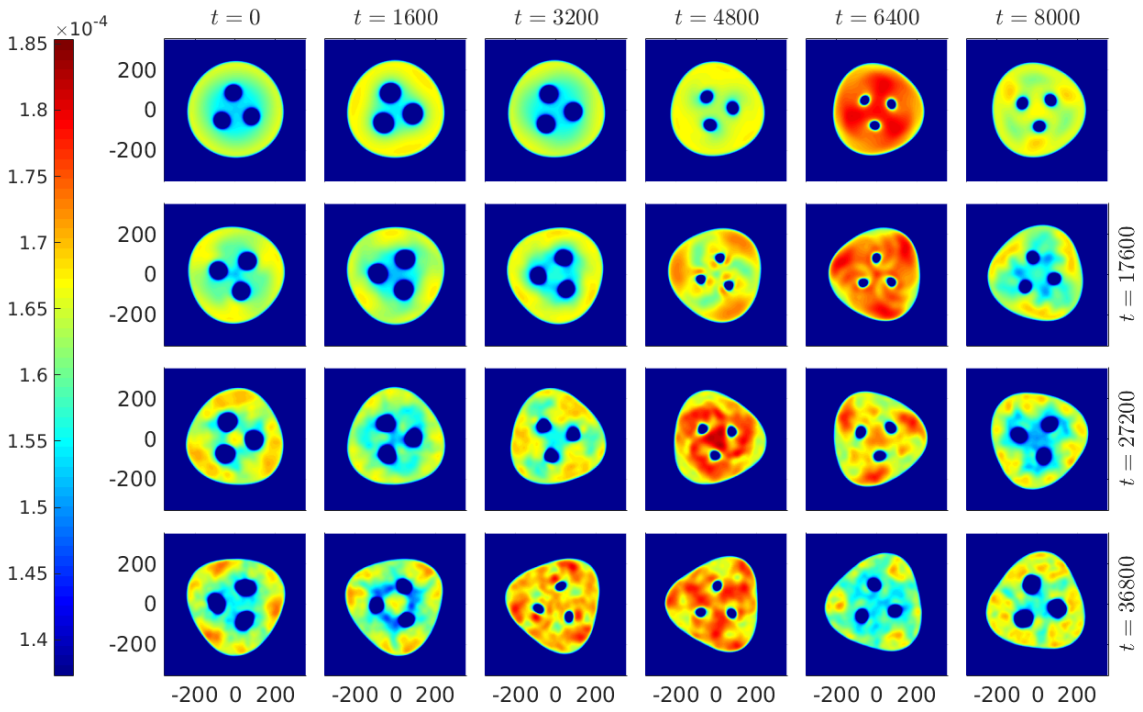

Figure 5.8: Real-time evolution of $m = 3$, $v = 10^{-4}\omega_0$ and $\omega_0 = 0.001$. The plot in the top left is at $t = 0$ directly after release. Each further plot from the top left to the bottom right evolves the system by $\Delta t = 1800$.

Chapter 6 | Conclusion

In this thesis, the formation of quasi-two-dimensional droplets and their rotational stability and dynamics were studied in a mean-field imaginary and real-time approach. The work is mostly numerical, using the extended Gross-Pitaveskii equation, supplemented by some analytical calculations regarding the required pressure equilibrium and real-time stability requirements.

The formation of quasi-two-dimensional droplets was confirmed in Sec.5.1, where we chose $\delta g \ll g$ to stay in the range of validity of the derivation of the quasi-two-dimensional LHY-correction, which uses $\sqrt{g_{11}g_{22}} = -g_{12}$. The self-bound droplet forms a true ground state of the system, with constant particle density n independent of the number of particles N in the system. Furthermore, we can expect from Fig. (4.1) that self-bound droplets in lower dimensionality can form over a wider range of parameters, than their three-dimensional counterparts. So far, experiments were only done on three-dimensional droplets, thus inviting for a study in lower dimensionality, by squeezing the system with a trap in one axis, while tuning the scattering length of both components via Feshbach-resonances [61].

Due to the self-bound nature, rotational dynamics of the system offer a variety of configurations that can be studied. We focused on the real-time stability and dynamics of the unit vortex in Sec. 5.2 and Sec. 5.3.1, by first showing that the expectation value of angular momentum is conserved in real-time independent of the external or particle-particle potential. This gives us an important benchmark for further results. Realising the importance of the trap-opening speed on the initially trapped ground state in Fig. (5.3), we investigate the real-time evolution of different opening speeds, directly after full release. Fig. (5.4) shows the formation of expanding rings after release for a non-adiabatic trap opening, which yields unphysical results where the GPe breaks down and does not conserve angular momentum. Despite total angular momentum being conserved over time, it is not confirmed whether both rings contain their angular momentum and will be subject of future work. More importantly, we found a similarity to the breathing mode [39] for stable solutions, where depending on the trap opening speed, the amplitude and frequency of oscillation for droplet size and vortex core change.

In Sec. 5.3.2 we repeated the study on stability and rotational dynamics for systems with multiple single-quantised vortices. We found in Fig. (5.7) that a higher number of vortices m requires a lower trap opening speed v. Additionally, while gathering the data, we found that a higher m requires a higher number of particles N to keep the system stable, which is in agreement with [57]. In the last paragraph of Sec. 5.3.2 we described the rotational dynamics of a system with $m = 3$, $v = 10^{-4}\omega_0$ and $\omega_0 = 0.001$ and found that added to the previously observed effects occurring, the droplet changes its shape to m-fold discrete rotational symmetry given enough time. Similar effects occur in all studied systems and can be seen in [59].

Considering the possible experimental realisation, we need to add that the creation of self-bound vortex solutions may prove to be difficult. Our initial calculation shows that the angular momentum is conserved for any potential. However, this excludes perturbation or particle losses. The former are never fully avoided in an experimental setup, the latter are inherent for self-bound droplets as shown by Petrov in [27]. We show a possibility to stabilise the system against perturbations via a non-monotonous potential in [60].

On more speculative grounds, another possible direction for further investigation emerges when drawing an analogy to fermionic density-functional theory: In that case, the potentials used in practical implementations can be affected by self-interaction contributions. How this issue correlates to the bosonic LHY-correction applied in this thesis is unclear at present stage, and poses a question for future research.

Due to the novelty of self-bound droplets, this research area offers a plethora of possible studies in the continuation and advancement of this work. An analytical investigation of the breathing behaviour, density waves and shape transform of stable vortex solutions, similar to as it was done for a trapped system [62–65], will be useful in advancing the understanding of the effect and finding analogies to already fully understood classical hydrodynamical systems [66]. Furthermore, we can extend this thesis, by considering dipolar interaction, or extending the study to a fully three-dimensional system.

Introducing a periodical change in scattering length over time can prove to be interesting, similar to [67], where a condensate surrounded by a ring-trap potential was modulated over time. The resulting firework-like jet-emission were then simulated using the mean field Gross-Pitaevskii equation and brought into connection with density waves within the condensate [68]. However, the logarithmic shape of the LHY-correction varies widely from a pure mean field approach so that an analytical and numerical study of such a system can shed new light on the underlying physical mechanisms.

Bibliography

[1] Bose, S. *Z. Phys.* **26,** 178–181 (1924).

[2] Einstein, A. *Sitzungsber. K. Preuss. Akad. Wiss.* **12,** 261 (1924).

[3] Einstein, A. *Sitzungsber. K. Preuss. Akad. Wiss.* **1,** 3 (1925).

[4] Ketterle, W. *Rev. Mod. Phys.* **74,** 1131–1151 (2002).

[5] Cornell, E. A. & Wieman, C. E. *Rev. Mod. Phys.* **74,** 875–893 (2002).

[6] Ensher, J. R., Jin, D. S., Matthews, M. R., Wieman, C. E. & Cornell, E. A. *Phys. Rev. Lett.* **77,** 4984–4987 (1996).

[7] Davis, K. B., Mewes, M.-O., Joffe, M. A., Andrews, M. R. & Ketterle, W. *Phys. Rev. Lett.* **74,** 5202–5205 (1995).

[8] Anderson, M. H., Ensher, J. R., Matthews, M. R., Wieman, C. E. & Cornell, E. A. *Science* **269,** 198–201 (1995).

[9] Davis, K. B. *et al.* **75,** 3969–3973 (1995).

[10] Bradley, C. C., Sackett, C. A. & Hulet, R. G. *Phys. Rev. Lett.* **78,** 985–989 (1997).

[11] Gross, E. P. *Nuovo Cimento* **20,** 454–477 (1960).

[12] Pitaevskii, L. P. *Sov. Phys. JETP* **13,** 451 (1961).

[13] Bogoliubov, N. *J. Phys* **11,** 23 (1947).

[14] Recati, A., Pavloff, N. & Carusotto, I. *Phys. Rev. A* **80,** 043603 (2009).

[15] Fiszdon, W. *J. Journal of Fluid Mechanics* **233,** 691–692 (1991).

[16] Feynman, R. in (ed Gorter, C.) 17–53 (Elsevier, 1955).

[17] Milošević, M. V. & Peeters, F. M. *Phys. Rev. B* **68,** 024509 (2003).

[18] Abo-Shaeer, J. R., Raman, C., Vogels, J. M. & Ketterle, W. *Science* **292,** 476–479 (2001).

[19] London, F. *Phys. Rev.* **54,** 947–954 (1938).

[20] Tisza, L. *Phys. Rev.* **72,** 838–854 (1947).

[21] Butts, D. & S Rokhsar, D. *Nature* **397,** 327–9 (1999).

[22] Matthews, M. R. *et al. Phys. Rev. Lett.* **83,** 2498–2501 (1999).

[23] Williams, J. & Holland, M. *Nature* **401,** 568 (1999).

[24] Christensson, J. *et al. New J. Phys.* **10,** 033029 (2008).

[25] Leanhardt, A. E., Shin, Y., Kielpinski, D., Pritchard, D. E. & Ketterle, W. *Phys. Rev. Lett.* **90,** 140403 (2003).

[26] Schweikhard, V. *et al. Phys. Rev. Lett.* **93,** 210403 (2004).

[27] Petrov, D. *Phys. Rev. Lett.* **115,** 155302 (2015).

[28] Lee, T. D., Huang, K. & Yang, C. N. *Phys. Rev.* **106,** 1135–1145 (1957).

[29] Schmitt, M., Wenzel, M., Böttcher, F., Ferrier-Barbut, I. & Pfau, T. *Nature* **539,** 259 (2016).

[30] Kadau, H. *et al. Nature* **530,** 194 (2016).

[31] Ferrier-Barbut, I., Kadau, H., Schmitt, M., Wenzel, M. & Pfau, T. *Phys. Rev. Lett.* **116,** 215301 (2016).

[32] Cabrera, C. R. *et al. Science* **359,** 301–304 (2018).

[33] Semeghini, G. *et al. Phys. Rev. Lett.* **120,** 235301 (2018).

[34] Petrov, D. S. & Astrakharchik, G. E. *Phys. Rev. Lett.* **117,** 100401 (2016).

[35] Zin, P., Pylak, M., Wasak, T., Gajda, M. & Idziaszek, Z. *Phys. Rev. A* **98,** 051603 (2018).

[36] Pauli, W. *Phys. Rev.* **58,** 716–722 (1940).

[37] Feynman, R. P. *Statistical Mechanics - A Set of Lectures* (Benjamin Advanced Book, 1972).

[38] Pitaevskii, L. & Stringari, S. *Bose-Einstein Condensation* (2003).

[39] Pethick, C. J. & Smith, H. *Bose–Einstein Condensation in Dilute Gases* 2nd ed. (Cambridge University Press, 2008).

[40] Huang, K. & Yang, C. N. *Phys. Rev.* **105,** 767–775 (1957).

[41] Larsen, D. M. *Ann. Phys. (N. Y.)* **24,** 89 (1963).

[42] Ilg, T., Kumlin, J., Santos, L., Petrov, D. S. & Büchler, H. P. *Phys. Rev. A* **98,** 051604 (2018).

[43] Ginzburg, V. & Pitaevskii, L. *Sov. Phys. JETP* **7,** 858 (1958).

[44] Lundh, E. *Phys. Rev. A* **65,** 043604 (2002).

[45] Engels, P., Coddington, I., Haljan, P. C., Schweikhard, V. & Cornell, E. A. *Phys. Rev. Lett.* **90,** 170405 (2003).

[46] Lundh, E., J. Pethick, C. & Smith, H. *Phys. Rev. A.* **55,** 2126–2131 (1997).

[47] Chin, S. A. & Krotscheck, E. *Phys. Rev. E* **72,** 036705 (2005).

[48] Chin, C., Grimm, R., Julienne, P. & Tiesinga, E. *Rev. Mod. Phys.* **82,** 1225–1286 (2010).

[49] Chin, S. A. & Krotscheck, E. *Phys. Rev. E* **72,** 036705 (2005).

[50] Saarikoski, H., Reimann, S. M., Harju, A. & Manninen, M. *Rev. Mod. Phys.* **82,** 2785–2834 (2010).

[51] Aichinger, M., Chin, S. A. & Krotscheck, E. *Comput. Phys. Commun* **171,** 197–207 (2005).

[52] Petrov, D. S., Holzmann, M. & Shlyapnikov, G. V. *Phys. Rev. Lett.* **84,** 2551–2555 (2000).

[53] Petrov, D. S. & Astrakharchik, G. E. *Phys. Rev. Lett.* **117,** 100401 (2016).

[54] Lundh, E., J. Pethick, C. & Smith, H. *Phys. Rev. A* **55,** 2126–2131 (1997).

[55] Kavoulakis, G. M., Mottelson, B. & Pethick, C. J. *Phys. Rev. A* **62,** 063605 (2000).

[56] Rosenbusch, P. *et al. Phys. Rev. Lett.* **88,** 250403 (2002).

[57] Li, Y. *et al. Phys. Rev. A* **98,** 063602 (2018).

[58] Cidrim, A., dos Santos, F. E. A., Henn, E. A. L. & Macrı, T. *Phys. Rev. A* **98,** 023618 (2018).

[59] Stürmer, P. *Rotational dynamics of vortices in quasi-two-dimensional droplets* `https://bit.ly/2Wny6zR`.

[60] Nilsson Tengstrand, M., Stürmer, P. & Reimann, S. M. `arXiv:1905.09738` (2019).

[61] Cabrera, C. *et al. Science* **359,** 301–304 (2018).

[62] Stringari, S. *Phys. Rev. Lett.* **77,** 2360–2363 (1996).

[63] Simula, T. P., Mizushima, T. & Machida, K. *Phys. Rev. A* **78,** 053604 (2008).

[64] Simula, T. P., Mizushima, T. & Machida, K. *Phys. Rev. Lett.* **101,** 020402 (2008).

[65] Fetter, A. L. & Svidzinsky, A. A. *Journal of Physics: Condensed Matter* **13,** R135–R194 (2001).

[66] Jørgensen, N. B., Bruun, G. M. & Arlt, J. J. *Phys. Rev. Lett.* **121,** 173403 (2018).

[67] Clark, L. W., Gaj, A., Feng, L. & Chin, C. *Nature* **551,** 356 (2017).

[68] Fu, H. *et al. Phys. Rev. Lett.* **121,** 243001 (2018).

[69] Eriksson, G. personal communication. 2018.

[70] Nilsson Tengstrand, M. personal communication. 2019.

Appendices

Chapter A | Derivation of the Gross-Pitaevskii equation

We derive the GPe in Ch. 2.2 starting from Eq. (2.4), following [38, 39]:

$$i\hbar\frac{\partial}{\partial t}\hat{\Psi}(\mathbf{r},t) = \left[\hat{\Psi}(\mathbf{r},t), \hat{H}\right] \tag{A.1}$$

Using the commutation relations

$$\left[\hat{\Psi}(\mathbf{r},t), \hat{\Psi}^\dagger(\mathbf{r}')\right] = \delta(\mathbf{r}-\mathbf{r}',t) \text{ and} \tag{A.2}$$

$$\left[\hat{\Psi}(\mathbf{r},t), \hat{\Psi}(\mathbf{r}',t)\right] = 0 \tag{A.3}$$

and for the many-body Hamiltonian

$$\hat{H} = \int d\mathbf{r}\, \left(\frac{\hbar^2}{2m}\boldsymbol{\nabla}\hat{\Psi}^\dagger(\mathbf{r},t)\boldsymbol{\nabla}\hat{\Psi}(\mathbf{r},t)\right) + \frac{1}{2}\int d\mathbf{r}'\, d\mathbf{r}\, \hat{\Psi}^\dagger(\mathbf{r},t)\hat{\Psi}^\dagger(\mathbf{r}',t)V\left(\mathbf{r}'-\mathbf{r},t\right)\hat{\Psi}(\mathbf{r},t)\hat{\Psi}(\mathbf{r}',t). \tag{A.4}$$

If we now use Eq. (A.1), we will get two parts of an equation on the righthand side, $\hat{\Psi}\hat{H}$ and $\hat{H}\hat{\Psi}$. Using

$$\hat{\Psi}(\mathbf{r},t) = \sum_{\mathbf{p}} \hat{a}_{\mathbf{p}} \frac{1}{\sqrt{V}} \exp\left(\frac{i\mathbf{p}\cdot\mathbf{r}}{\hbar}\right) \tag{A.5}$$

one can rewrite Eq. (A.4) into

$$\hat{H} = \sum \frac{p^2}{2m}\hat{a}^\dagger_{\mathbf{p}}\hat{a}_{\mathbf{p}} + \frac{1}{2V}\sum V_{\mathbf{q}}\hat{a}_{\mathbf{p}_1+\mathbf{q}}\hat{a}^\dagger_{\mathbf{p}_2-\mathbf{p}}\hat{a}_{\mathbf{p}_1}\hat{a}_{\mathbf{p}_2} \tag{A.6}$$

At first $\hat{\Psi}\hat{H}$ is taken care of and turns into [38, 39]

$$\left[\sum \hat{a}_{\mathbf{p}}\frac{1}{\sqrt{V}}\exp\left(\frac{i\mathbf{p}\cdot\mathbf{r}}{\hbar}\right)\right]\left[\sum \frac{p^2}{2m}\hat{a}^\dagger_{\mathbf{p}}\hat{a}_{\mathbf{p}} + \frac{1}{2V}\sum V_{\mathbf{q}}\hat{a}_{\mathbf{p}_1+\mathbf{q}}\hat{a}^\dagger_{\mathbf{p}_2-\mathbf{p}}\hat{a}_{\mathbf{p}_1}\hat{a}_{\mathbf{p}_2}\right] \tag{A.7}$$

while $\hat{H}\hat{\Psi}$ is symmetric to latter expression. One can immediately identify two different terms, separated by the plus sign, which we treat separately.

$$\sum \hat{a}_{\mathbf{p}}\frac{1}{\sqrt{V}}\exp\left(\frac{i\mathbf{p}\cdot\mathbf{r}}{\hbar}\right)\sum \frac{p^2}{2m}\hat{a}^\dagger_{\mathbf{p}}\hat{a}_{\mathbf{p}} \tag{A.8}$$

Also considering the symmetric part from $\hat{H}\hat{\Psi}$ and for simplicity ignoring every non-operator part of the expression, we obtain

$$\begin{aligned}\hat{a}_{\mathbf{p}}\hat{a}_{\mathbf{p}}^{\dagger}\hat{a}_{\mathbf{p}} - \hat{a}_{\mathbf{p}}^{\dagger}\hat{a}_{\mathbf{p}}\hat{a}_{\mathbf{p}} &= \\ &= \left[\hat{a}_{\mathbf{p}}, \hat{a}_{\mathbf{p}}^{\dagger}\hat{a}_{\mathbf{p}}\right] \\ &= \left[\hat{a}_{\mathbf{p}}, \hat{a}_{\mathbf{p}}^{\dagger}\right]\hat{a}_{\mathbf{p}} + \hat{a}_{\mathbf{p}}^{\dagger}\left[\hat{a}_{\mathbf{p}}, \hat{a}_{\mathbf{p}}\right] \\ &= \hat{a}_{\mathbf{p}} + 0 \\ &= \hat{a}_{\mathbf{p}} \end{aligned} \tag{A.9}$$

Inserting this into the original equation, gives

$$\begin{aligned}\sum \frac{p^2}{2m}\hat{a}_{\mathbf{p}}\frac{1}{\sqrt{V}}\exp\left(\frac{i\mathbf{p}\cdot\mathbf{r}}{\hbar}\right) &= \\ &= -\frac{\hbar^2\boldsymbol{\nabla}^2}{2m}\hat{\Psi}(\mathbf{r},t)\end{aligned} \tag{A.10}$$

With use of Eq. (A.3), which is analogously applicable to annihilation and creation operators. The last part of the equation turns into [38, 39]:

$$\begin{aligned}\hat{a}_{\mathbf{p}_1}\hat{a}_{\mathbf{p}_1+\mathbf{q}}\hat{a}_{\mathbf{p}_2-\mathbf{q}}\hat{a}_{\mathbf{p}_1}\hat{a}_{\mathbf{p}_2} - \hat{a}_{\mathbf{p}_1+\mathbf{q}}\hat{a}_{\mathbf{p}_2-\mathbf{q}}\hat{a}_{\mathbf{p}_1}\hat{a}_{\mathbf{p}_2}\hat{a}_{\mathbf{p}_1} &= \\ &= \left[\hat{a}_{\mathbf{p}_1}, \hat{a}_{\mathbf{p}_1+\mathbf{q}}\hat{a}_{\mathbf{p}_2-\mathbf{q}}\hat{a}_{\mathbf{p}_1}\hat{a}_{\mathbf{p}_2}\right] \\ &= \left[\hat{a}_{\mathbf{p}_1}, \hat{a}_{\mathbf{p}_1+\mathbf{q}}\hat{a}_{\mathbf{p}_2-\mathbf{q}}\hat{a}_{\mathbf{p}_1}\right]\hat{a}_{\mathbf{p}_2} + \hat{a}_{\mathbf{p}_1}, \hat{a}_{\mathbf{p}_1+\mathbf{q}}\hat{a}_{\mathbf{p}_2-\mathbf{q}}\left[\hat{a}_{\mathbf{p}_1}, \hat{a}_{\mathbf{p}_2}\right]\end{aligned} \tag{A.11}$$

$$= \dots$$

$$\begin{aligned}\text{with } \left[\hat{a}_{\mathbf{p}_1}, \hat{a}_{\mathbf{p}_1+\mathbf{q}}\hat{a}_{\mathbf{p}_2-\mathbf{q}}\hat{a}_{\mathbf{p}_1}\right] &= \left[\hat{a}_{\mathbf{p}_1}, \hat{a}_{\mathbf{p}_1+\mathbf{q}}\hat{a}_{\mathbf{p}_2-\mathbf{q}}\right]\hat{a}_{\mathbf{p}_1} + \hat{a}_{\mathbf{p}_1+\mathbf{q}}\hat{a}_{\mathbf{p}_2-\mathbf{q}}\left[\hat{a}_{\mathbf{p}_1}, \hat{a}_{\mathbf{p}_1}\right] \\ &= \dots\end{aligned} \tag{A.12}$$

$$\begin{aligned}\text{with } \left[\hat{a}_{\mathbf{p}_1}, \hat{a}_{\mathbf{p}_1+\mathbf{q}}\hat{a}_{\mathbf{p}_2-\mathbf{q}}\right] &= \left[\hat{a}_{\mathbf{p}_1}, \hat{a}_{\mathbf{p}_1+\mathbf{q}}\right]\hat{a}_{\mathbf{p}_2-\mathbf{q}} + \hat{a}_{\mathbf{p}_1+\mathbf{q}}\left[\hat{a}_{\mathbf{p}_1}, \hat{a}_{\mathbf{p}_2-\mathbf{q}}\right] \\ &= \hat{a}_{\mathbf{p}_2-\mathbf{q}}\end{aligned} \tag{A.13}$$

Eq. (A.13) in Eq. (A.12) in Eq. (A.11) gives

$$\dots = \hat{a}_{\mathbf{p}_2-\mathbf{q}}\hat{a}_{\mathbf{p}_1}\hat{a}_{\mathbf{p}_2} \tag{A.14}$$

Inserting this into Eq. (A.6), gives

$$\frac{1}{2V}\frac{1}{\sqrt{V}}\sum V_{\mathbf{q}}\hat{a}_{\mathbf{p}_2-\mathbf{q}}\hat{a}_{\mathbf{p}_1}\hat{a}_{\mathbf{p}_2}\exp\left(\frac{i\mathbf{p}\cdot\mathbf{r}}{\hbar}\right) = \left[\int d\mathbf{r}'\,\hat{\Psi}^{\dagger}(\mathbf{r}',t)V(\mathbf{r}'-\mathbf{r})\hat{\Psi}(\mathbf{r}',t)\right]\hat{\Psi}(\mathbf{r},t) \tag{A.15}$$

As we previously ignored the treatment of any external potential, we are able to add this in the final outcome

$$i\hbar\frac{\partial}{\partial t}\Psi(\mathbf{r},t) = \left[-\frac{\hbar^2\boldsymbol{\nabla}^2}{2m} + V_{ext}(\mathbf{r},t) + \int d\mathbf{r}'\,\hat{\Psi}^{\dagger}(\mathbf{r}',t)V(\mathbf{r}'-\mathbf{r})\hat{\Psi}(\mathbf{r}',t)\right]\hat{\Psi}(\mathbf{r},t) \tag{A.16}$$

We are now allowed to replace the field operator $\hat{\Psi}$ with the classical field Ψ_0, if Eq. (2.3) is valid

$$i\hbar\frac{\partial}{\partial t}\Psi_0(\mathbf{r},t) = \left(-\frac{\hbar^2\boldsymbol{\nabla}^2}{2m} + V_{ext}(\mathbf{r},t) + g|\Psi_0(\mathbf{r},t)|^2\right)\Psi_0(\mathbf{r},t) \tag{A.17}$$

Chapter B | Comparison of rotational dynamics between mean field and LHY-fluid

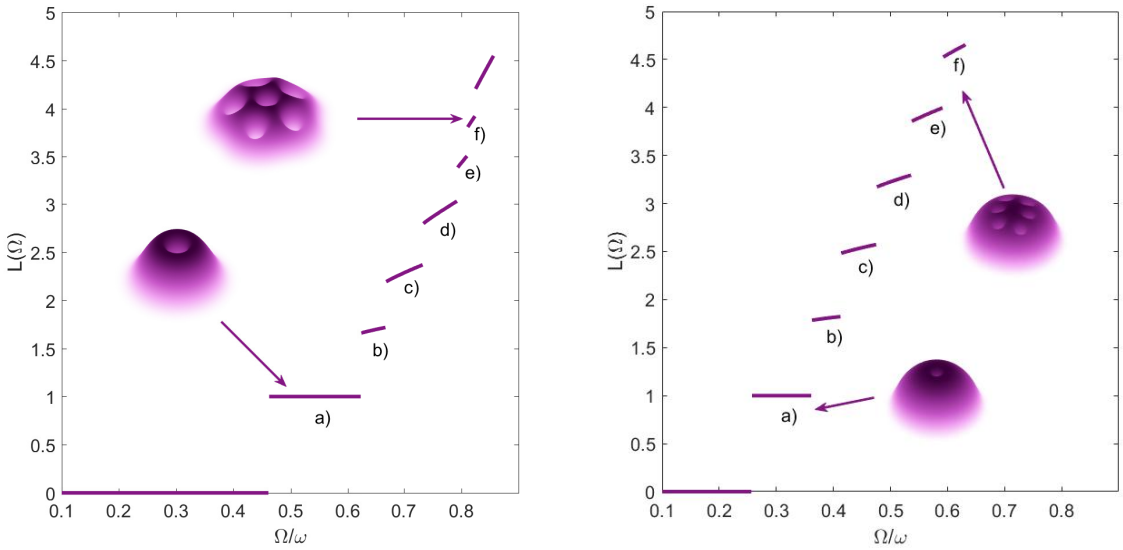

Figure B.1: Left: $L(\Omega)$ for mean field interaction
Right: $L(\Omega)$ for pure LHY-interaction without mean field

Comparing both, purely mean field interaction and LHY-fluid as in Sec. 5.2 we find that the critical angular momentum is lowered for the LHY-fluid which corresponds to the generally weaker LHY-interaction than mean field. However, we find that the vortex core size is lower for the LHY-fluid, but for a weaker interaction it should increase in size. In the LHY-fluid the different vortex states ascend in $L(\Omega)$ is less steep compared to purely mean field as well as each state exists with less variation in Ω. Additionally, we find a different vortex formation for $m = [5, 6]$. It is however unclear if this whether due to peculiar form of the LHY-correction or if the true ground state for the system was not found and the vortices for the LHY-system represent an excited state.

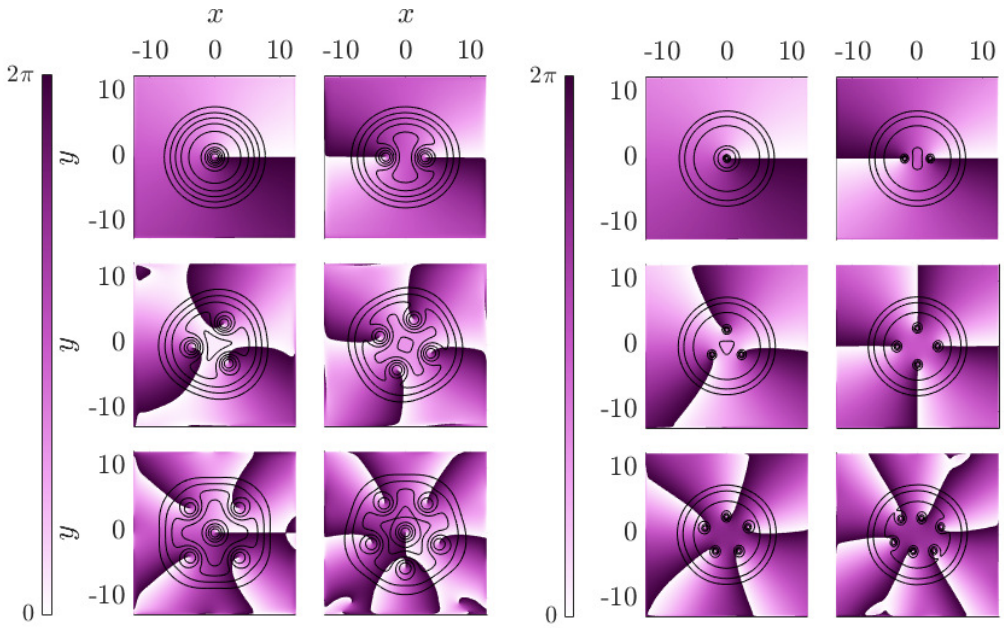

Figure B.2: Left: $L(\Omega)$ for mean field interaction
Right: $L(\Omega)$ for pure LHY-interaction without mean field

Chapter C | Derivation of the three-dimensional LHY-correction to the mean field energy

We complete the derivation of the LHY-correction to the mean field energy in Ch. 2.3.2, continuing from Eq. (2.21), following [38]:

$$|u_{\mathbf{p}}|^2 - |v_{-\mathbf{p}}|^2 = 1 \tag{C.1}$$

Is fulfilled when

$$u_{\mathbf{p}} = \cosh \alpha_{\mathbf{p}} \text{ and } v_{\mathbf{p}} = \sinh \alpha_{\mathbf{p}}. \tag{C.2}$$

We then choose $\alpha_{\mathbf{p}}$ such that $\hat{b}^\dagger_{\mathbf{p}}\hat{b}^\dagger_{\mathbf{p}}$ and $\hat{b}_{\mathbf{p}}\hat{b}_{\mathbf{p}}$ vanish in the Hamiltonian in Eq. (2.17). This is solved for:

$$\frac{gn}{2}\left(|u_{\mathbf{p}}|^2 - |v_{-\mathbf{p}}|\right) + \left(\frac{p^2}{2m} + gn\right) u_{\mathbf{p}} v_{-\mathbf{p}} = 0. \tag{C.3}$$

We solve Eq. (C.3) with help of $\cosh 2\alpha = \cosh \alpha^2 + \sinh \alpha^2$ and $\sinh 2\alpha = 2 \cosh \alpha \sinh \alpha$, which gives us:

$$\coth 2\alpha_{\mathbf{p}} = \pm \left(\frac{p^2/2m + gn}{2\epsilon(\mathbf{p})} \pm \frac{1}{2}\right)^{1/2}. \tag{C.4}$$

where $\epsilon(\mathbf{p})$ is the dispersion relation in Eq. (2.24). Eq. (C.4) reduces the Hamiltonian $\hat{H}$ to Eq. (2.22).

In the following we calculate the phase space integral mentioned around Eq. (2.23) [69]:

$$E_0 = \frac{gN^2}{2V} + \frac{1}{2}\sum_{\mathbf{p}\neq\mathbf{0}} \left[\left(\frac{gn}{m} p^2 + \left(\frac{p^2}{2m}\right)^2 \right)^{1/2} - gn - \frac{p^2}{2m} + \frac{m(gn)^2}{p^2} \right]$$

with $p = \sqrt{2mgn}x$ and $dp/dx = \sqrt{2mgn}$

$$\begin{aligned} E_0 &= \frac{gN^2}{2V} + \frac{1}{2}\sum_{\mathbf{p}\neq\mathbf{0}} \left[\left(2(gn)^2x^2 + (gn)^2x^4\right)^{1/2} - gn - gnx^2 + \frac{m(gn)^2}{2mgnx^2} \right] \\ &= \frac{gN^2}{2V} + \frac{1}{2}\sum_{\mathbf{p}\neq\mathbf{0}} gn \left[x(2+x^2)^{1/2} - 1 - x^2 + \frac{1}{2x^2} \right]. \end{aligned}$$

Turning the sum over the phase space into a phase space integral gives:

$$\begin{aligned}
E_0 &= \frac{gN^2}{2V} + \frac{1}{2}\frac{gnV}{(2\pi\hbar)^3}\int_{\mathbb{R}^3} d^3p\,\left[x(2+x^2)^{1/2} - 1 - x^2 + \frac{1}{2x^2}\right] \\
&= \frac{gN^2}{2V} + \frac{1}{2}\frac{gN}{(2\pi\hbar)^3}\int_0^\infty dp \int_0^\pi d\,\Theta \int_0^{2\pi} d\phi\, p^2 \sin\Theta \left[x(2+x^2)^{1/2} - 1 - x^2 + \frac{1}{2x^2}\right] \\
&= \frac{gN^2}{2V} + \frac{gN}{2}\frac{4\pi}{(2\pi\hbar)^3}(2mgn)^{3/2}\int_0^\infty dx\, x^2 \left[x(2+x^2)^{1/2} - 1 - x^2 + \frac{1}{2x^2}\right].
\end{aligned}$$

Where the integrand is a positive monotonusly decreasing function with $f(0) = 1/2$, thus the integral converges to $\approx \sqrt{128}/15$ and it follows:

$$\begin{aligned}
E_0 &= \frac{gN^2}{2V} + \frac{\sqrt{128}}{15}\frac{gN}{2}\frac{(2mgn)^{3/2}}{2\pi^2\hbar^3} \\
&= \frac{gN^2}{2V}\left(1 + \frac{128}{15\sqrt{\pi}}\sqrt{a^3 n}\right).
\end{aligned}$$

which matches Eq. (2.25).

Chapter D | Conservation of angular momentum for an arbitrary real interaction potential

We show the conservation of angular momentum in real-time for a zeroth-order mean-field and quasi-two-dimensional LHY-correction, which is used as a benchmark for the physicality of our results. The calculation was double checked by [70] as it will be used in [60].

The time derivative of the angular momentum L_z is given by:

$$\frac{d}{dt}\langle L_z\rangle = \frac{d}{dt}\int d^2\,\mathbf{r}(\Psi_0^* L_z \Psi_0) = \int d^2\,\mathbf{r}\left[(\partial_t\Psi_0^*)\,L_z\Psi_0 + \Psi_0^*\,(\partial_t L_z)\,\Psi_0 + \Psi_0^* L_z\,(\partial_t\Psi_0)\right]. \quad \text{(D.1)}$$

Where $\partial_t L_z = 0$ on the right-hand side. Additionally, we can use the GPe for the remaining two terms, such that

$$\partial_t\Psi_0 = -iA\Psi_0, \quad \partial_t\Psi_0^* = i(A\Psi_0)^*, \quad \text{(D.2)}$$

where $A = -(1/2)\boldsymbol{\nabla}^2 + V_{trap} + V_{int}$, V_{trap} an arbitrary external trapping potential and V_{int} the aforementioned interaction potentials. Inserting this into Eq. (D.1) gives

$$\begin{aligned}\frac{d}{dt}\langle L_z\rangle &= i\int d^2\,\mathbf{r}\left[(A\Psi_0)^*\,L_z\Psi_0 + \Psi_0^* L_z\,(A\Psi_0)\right] = \\ &= i\int d^2\,\mathbf{r}\Bigg(\left(-\frac{1}{2}\boldsymbol{\nabla}^2\Psi_0^* L_z\Psi_0 + \frac{1}{2}\Psi_0^* L_z\boldsymbol{\nabla}^2\Psi_0\right) \\ &\quad + (V_{trap}\Psi_0^* L_z\Psi_0 - \Psi_0^* L_z V_{trap}\Psi_0) + (V_{int}\Psi_0^* L_z\Psi_0 - \Psi_0^* L_z V_{int}\Psi_0)\Bigg).\end{aligned} \quad \text{(D.3)}$$

With L_z in spatial representation for two-dimensional spherical coordinates:

$$L_z = -i\partial_\phi. \quad \text{(D.4)}$$

We know that the free particle must conserve angular momentum L_z, however, we can show by using integration by parts twice, that the first term in Eq. (D.3) indeed equals zero. Due to the similar shape of the remaining two terms, both follow the same transformation, where the right-hand side $\Psi_0^*\partial_\phi(\Psi_0 V)$ becomes

$$\Psi_0^*\partial_\phi(\Psi_0 V) = \Psi_0^*(\partial_\phi\Psi_0)V + \Psi_0^*(\partial_\phi V)\Psi_0 \quad \text{(D.5)}$$

and the first term cancels out the left-hand side, so that we remain with

$$\frac{d}{dt}\langle L_z\rangle = -\int d^2\,\mathbf{r}(\Psi_0^*\Psi_0\partial_\phi V_{trap} + \Psi_0^*\Psi_0\partial_\phi V_{int}). \quad \text{(D.6)}$$

While the trapping potential has an explicit space-dependency, this is not the case for the interaction potential. Thus angular momentum is conserved for a harmonic oscillator, but not for an anharmonic oscillator. Additionally we see that angular momentum is conserved for $m = [0, 1]$, however this is not trivially clear for $m > 1$. The quasi-two-dimensional interaction potential follows from Eq. (4.9) with $V = \partial_n E$ and consists out of three parts. The first are terms similar to zeroth-order mean field, with linear dependency on $kn = k|\Psi_0|^2 = k\Psi_0^*\Psi_0$, the second with quadratic dependcy on kn^2 and one term with $kn\ln(kn)$, where we replaced all the constants in Eq. (4.9) with k for simplicity. Starting with the zeroth-order mean field terms:

$$k\int d\,\phi\Psi_0^*\Psi_0\partial_\phi(\Psi_0^*\Psi_0) = k\left[\int d\,\phi\Psi_0^*\Psi_0\Psi_0\partial_\phi\Psi_0^* + \int d\,\phi\Psi_0^*\Psi_0\Psi_0^*\partial_\phi\Psi_0\right]. \tag{D.7}$$

We focus on the first term and use integration by parts

$$\int d\,\phi\Psi_0^*\Psi_0\Psi_0\partial_\phi\Psi_0^* = \left[|\Psi_0|^4\right]_0^{2\pi} - \int d\,\phi\Psi_0^*\left[\Psi_0\Psi_0\partial_\phi\Psi_0^* + 2\Psi_0^*\Psi_0\Psi_0^*\partial_\phi\Psi_0\right], \tag{D.8}$$

where the first term becomes zero and with the second term we see that

$$\int d\,\phi\Psi_0^*\Psi_0\Psi_0\partial_\phi\Psi_0^* = -\int d\,\phi\Psi_0^*\Psi_0\Psi_0^*\partial_\phi\Psi_0. \tag{D.9}$$

We insert this last expression into Eq. (D.7), thus the whole integral becomes zero and angular momentum is conserved.

$$\int d\,\phi\Psi_0^*\Psi\partial_\phi V_{int} = [\Psi_0^*\Psi_0 V]_0^{2\pi} - \int d\,\left((\partial_\phi\Psi_0^*)\Psi_0 + \Psi_0^*\partial_\phi\Psi_0\right). \tag{D.10}$$

We follow the same procedure for kn^2 and find that this also conserves angular momentum. For $\partial_\phi(kn\ln(kn))$ we find

$$\partial_\phi(k\Psi_0^*\Psi_0\ln(k\Psi_0^*\Psi_0)) = k\ln(k\Psi_0^*\Psi_0)\partial_\phi\Psi_0^*\Psi_0 + k\Psi_0^*\partial_\phi\Psi_0 + k\Psi_0\partial_\phi\Psi_0^*. \tag{D.11}$$

Where the last two terms are equal to the above zeroth-order mean field calculation. For the first term we follow again the calculation above and find that the $kn\ln(kn)$ also conserves angular momentum. Thus,

$$\frac{d}{dt}\langle L_z\rangle = 0, \tag{D.12}$$

for zeroth-order mean field and quasi-two-dimensional LHY-correction. Furthermore, is the two-dimensional LHY-correction often represented as $n\ln(n)$ and therefore, the angular momentum is also conserved in exact two dimensions. Additionally, it is save to assume that this is also the case for the three-dimensional LHY-correction in Eq. (2.25).